How Electrostatics Disrupts Gas-Solid Fluidized Bed Operations: A Review

Ghazal Saki Norouzi[1, *] - Heydar Rezaei[2]
[1] Chemical Engineering Department, Faculty of Petroleum and Chemical Engineering, Razi University, Kermanshah 67144- 14971, Iran.
[2] School of Chemical Engineering, College of Engineering, University of Tehran, 11155-4563, Tehran, Iran.

ABSTRACT

The dynamic dance of gas and solid particles in fluidized beds creates a hidden storm of electrostatic charges due to frequent collisions. This review dives into the world of these charges, exploring their generation mechanisms, potential trouble they can cause (think particle clumps, wall sheeting, fouling, and even sparks), and how we can keep them under control. By examining the fundamental principles, measurement techniques, and the complex interplay between electrostatics and fluid flow, we aim to spark ideas for future research and innovative solutions to unlock the full potential of fluidized bed reactors.

Keywords: Fluidized beds, Triboelectrification, Electrostatics, Hydrodynamics, Wall Sheeting, Fouling, Controlling Static Charge

1. INTRODUCTION

Fluidized beds have become pervasive in various chemical and physical processes [1]. This technology is adept at handling diverse feedstocks, fostering excellent gas-solid contact, efficient energy transfer, and uniform temperature distribution, as observed in gas-phase polyolefin production [2, 3]. Despite decades of research, challenges persist for researchers, process engineers, and scientists in the realm of fluidized beds. Frictional contacts between particles (both particle-particle and particle-wall) within fluidized-bed polymerization virtually guarantee the generation of electrostatic charges, which are generally undesirable [4]. The presence of electrostatic charges in gas-phase fluidized beds can significantly impact reactor operation. It is well-established that electrostatics also influences the hydrodynamics of these systems [5]. In a polymerization reactor, when the electrostatic charge on particles surpasses a critical threshold, the resulting electrostatic forces cause them to adhere to the reactor wall, forming sheets. This adhesion of catalyst and resin particles to the reactor wall is termed sheeting [4]. Drooling or dome sheeting manifests on the top of a reactor, in its conical dome section, or on its hemispherical head. Hendrickson [4] categorized sheets into two types: "warm sheets" and "cold sheets." "Warm sheets" arise from the adhesion of catalysts or catalyst-rich fines to reactor walls. They comprise a core of fused polymer with an outer surface of granular polymer fused onto the core. The "hairy" appearance of the sheet edges stems from the oriented strands of fused polymer. "Cold sheets" form through the adherence of polymer particles, rather than catalyst particles, to reactor walls. As polymerization progresses, the adhered particles heat up, potentially reaching the sintering temperature. This leads to the formation of sintering sheets without the excessively high reactor wall temperatures or "hairy" look associated with "warm sheets."

Insufficient mitigation strategies can lead to sheeting problems in commercial gas-phase polyolefin production reactors [6]. This issue results in the formation of large, solid polymer masses on the reactor walls, potentially reaching dimensions of several square meters and centimeters in thickness [7]. As depicted in Figure 1, this typically occurs around an elevation of 1/4 to 3/4 of the reactor diameter above the fluidization gas distributor plate. These solid masses (sheets) can detach from the walls within the reaction compartment, disrupting fluidization, obstructing the product outlet, and ultimately forcing an economically detrimental reactor shutdown [8, 4, 9].

Previous research has extensively explored the individual impacts of various parameters on fluidized beds. Overcoming operational challenges within gas-solid reactors hinges on a comprehensive understanding of both the reactor's fluid dynamics and the intricacies of bubble formation within the bed. To equip readers with a foundational grasp of these concepts, this paper reviews key electrostatic principles relevant to these systems. We then delve into the current state-of-the-art, examining the interplay between electrostatics and hydrodynamics, the critical factors involved, and potential control strategies.

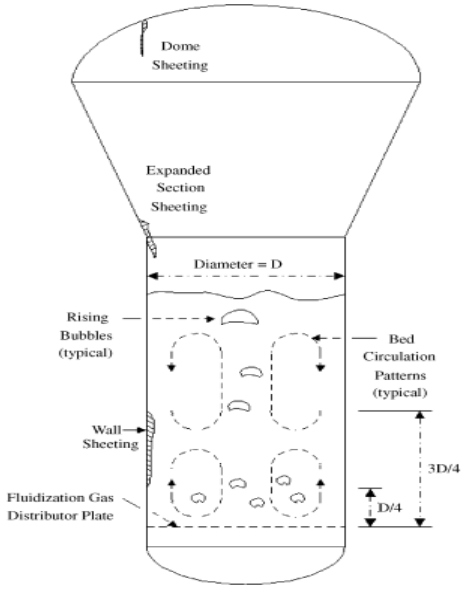

Fig. 1. A typical schematic of a polyolefin fluidized-bed reactor [4].

2. Fluidization: general principles

2.1 Fluidization Regimes *(Style: Times New Roman, 10pt, Bold, Title Case)*

As gas velocity and solid properties vary, the fluidized bed behaves differently. Figure 2 [10] illustrates a variety of fluidization regimes. Fluidization bed regimes include minimum fluidization, bubbling, turbulence, fast fluidization, and pneumatic conveying [11–14]. The types of regimes are mainly dependent on the fluidizing gas velocity, density, the particle size of the bed material, aspect ratio (height to the diameter of the bed), and reactor dimension [2,15, 16]. As the flow rate increases, frictional forces between particles and fluid increase. This occurs when the upward component of the force equals the particle weight. In this way, the bed reaches the minimum expansion condition. It is called minimum fluidization and has a corresponding minimum fluidization velocity, U_{mf}. When the velocity is increased further, some instability phenomena such as bubbling or turbulent fluidization may occur depending on the system geometry and particle properties. Gas bubbles tend to coalesce and grow in volume when traveling upward in a gas-solid system with high fluid velocity; if the bed is not wide enough, a gas bubble can take up the entire vessel cross-section, and the solid particles are lifted like pistons, which is why flat slugging is called that. Cohesive powders and coarse particles are both susceptible to this undesirable occurrence. Fluidized particles will exceed their terminal velocity if the flow rate is high enough. Turbulent motion of solid clusters and gas voids is observed instead of bubbles at the top of the bed. Figure 2.1E shows a turbulent bed under these conditions. Entrainment occurs when the gas velocity increases. As a result, we have a dispersed, diluted, or lean phase fluidized bed which amounts to pneumatic solid transport [10,17].

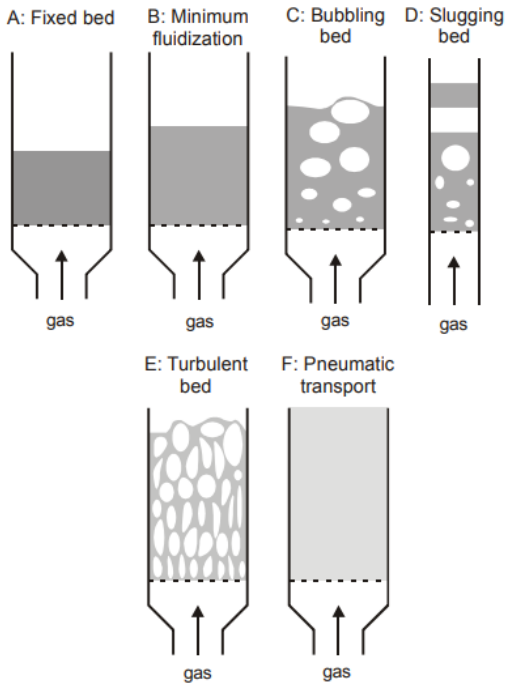

Fig. 2. A schematic of various fluidization regimes [2].

2.2 The Geldart Classification of Powders

Particle features play an essential role. According to their hydrodynamic behavior, particulate solid materials were grouped into four well-defined classes [18]. Based on this categorization, Figure 3 depicts the four different regions a fluidized air/solids system can go through at ambient conditions and speeds below $10*U_{mf}$, excluding pneumatic transport conditions. Based on the density of a solid ρ_s and mean particle size d_p, the graph indicates the type of fluidization that may occur. Additionally, it can predict bubble size, bubble velocity, and slug presence.

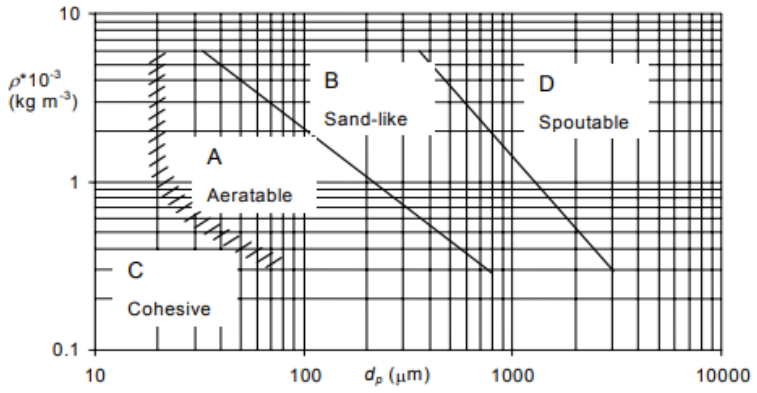

Fig. 3. the Geldart's particle classification [18].

3. MEASUREMENT

Electrostatic charge measurement allows fluidized bed properties characterization. As discussed above, in addition to particle agglomeration and electrostatic discharge, charge accumulation in the bed can cause reactor shutdowns [4,19,20]. Therefore, accurate monitoring of electrostatic charging is essential. It is worth noting that there are some valuable reviews available on measurement topics, such as Sun and Yan [19], which

provided a comprehensive overview of non-intrusive measurement techniques for monitoring gas-solid fluidized beds, so we focus only on the most significant ones.

There are two types of electrostatic sensors designed to measure electrostatic charges in fluidized beds: direct methods using Faraday cups, and indirect methods using collision (contact) or induction probes [21-25].

3.1 Faraday cups

Faraday cups are the most common method for measuring cumulative net charges on fluidized particles, and they are generally considered intrusive and offline devices [26-29]. Charged particles in fluidized beds through a sampling unit are poured into a Faraday cage, as illustrated in Figure 4 [30]. By this method, sampling from different regions of the fluidized bed is possible [31-37].

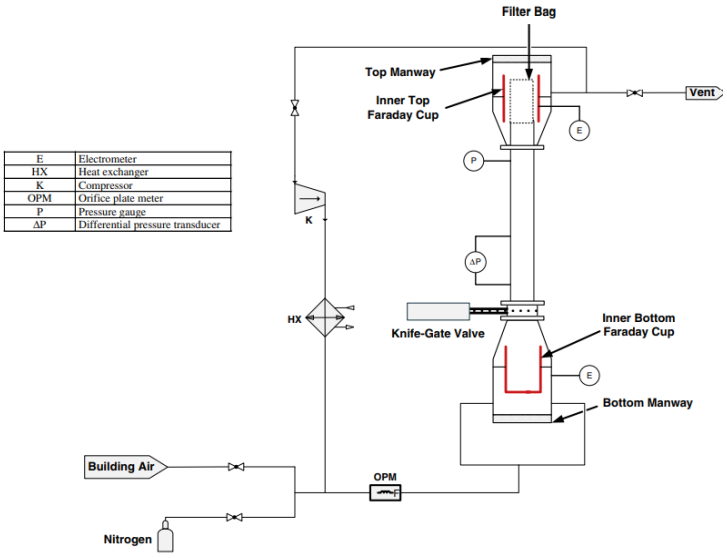

Fig. 4. Schematic diagram of faraday cups devised in a pilot plant fluidization system [30].

Because fluidized beds often encounter broad particle size distributions, detecting differential charging of particles of different sizes is crucial. Multi-compartment Faraday cup systems are used to determine the charge density of particles of various sizes sampled from fluidized beds. They separate particles of various charge densities into several Faraday cups arranged horizontally or vertically as shown in Figure 5 [32,38,39].

A non-intrusive Faraday cup was developed by Mehrani et al [25, 40]. The bed serves as the inner Faraday cup and the second column serves as the outer cup. Each section is made of a different material, as in Figure 6. The middle section is made of copper and connected to both ends of the Teflon sections. An electrometer is also attached to it to measure the charges induced by the column wall. To reduce particle entrainment, plexiglass is used in the top expanded section. To eliminate external electrical interference, the copper outer column is grounded. Faraday cups of this type do not have the drawbacks that conventional types do.

A common Faraday cup has some disadvantages that reduce measurement accuracy. In some cases, sampling from a fluidized bed might result in an additional charge due to particle handling. In addition, you might only be able to measure the net charge of the sample. To overcome these drawbacks some approaches have been undertaken. Utilizing Faraday cups equipped with filters to capture airborne particles and measure charge density in a fluidized bed. Take as large a sample as possible [41-43]. To determine the charge density, a Faraday cup should be constructed at both the top and bottom of the device. This will allow fine and coarse particles to be discharged directly into two separate cups [26,27,32,36,44]. A charge separator and a horizontal array Faraday cup system can also be used to determine the charge distribution of dropped particles [32,44]. Furthermore, since similar materials do not usually exchange much charge when in contact, the sampling unit (e.g., scooper, spoon) can be coated with the same material. The charge of polyamide powder fluidized in a steel column was measured using this technique by Ali et al. [45].

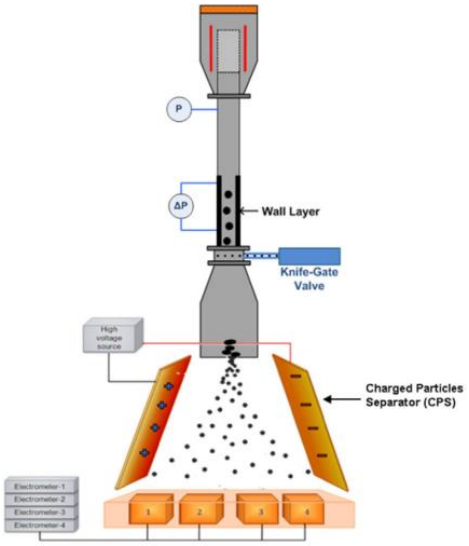

Fig. 5. Collecting the wall particles with the charged particle separator apparatus [32].

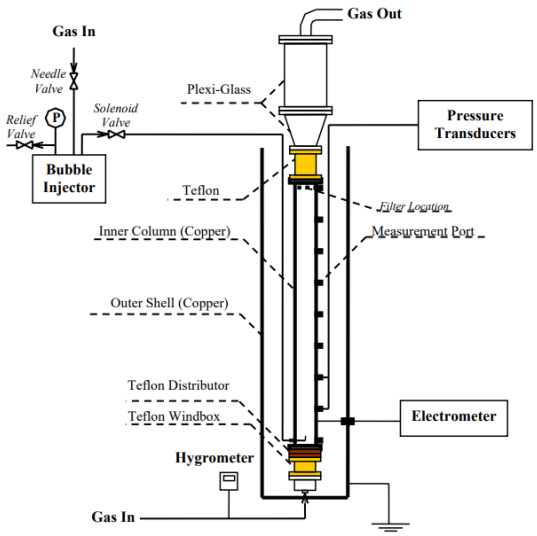

Fig. 6. Schematic diagram of experimental apparatus [25].

3.2 Electrostatic probes

Probe signals determine particle charging and hydrodynamics within the bed. An electrostatic probe produces an induced charge signal, a current signal, or a voltage signal. This reveals the charge level and charge distribution in a gas-solid fluidized bed [46-50].

3.2.1 Collision probes

Contact probes are inserted into the bed in the form of balls, hemispheres, or rods. Charges can be transferred directly between particles and probes, allowing direct measurement. Consequently, it is intrinsically intrusive and suitable for collecting electrostatic signals.

There are limitations to using a contact probe limitation including the generation of extra charges from particle collisions and adhesions, and the disturbance of the flow field [26]. As a result, contact probe signals should be analyzed qualitatively rather than quantitatively. However, contact probes are commonly used on gas-solid fluidized beds due to their ability to offer information regarding charge distribution, particle charge-

to-mass ratios, and even bubble-rising velocity [20, 51-54]. The properties of the particles and probe tip, e.g., work function, dielectric constant, electrical conductivity, particle density and size distribution, probe tip size and shape, affect current signals [55]. For a given combination of a probe and a bed material, the average magnitude of electrical current from collision probes depends not only on the charge density of particles colliding with the probe but also on the particle velocity and collision frequency, because charge transfer from charged particles to the probe is a function of the relative velocity or contact time of the contacting surfaces [56].

3.2.2 Induction Probes

Induction sensors are independent of net charge accumulation, as is the case with contact probes. Electrostatic signal processing can characterize a solid's velocity and relative concentration. As particles move around a rising bubble, the interaction between them is stronger than in the emulsion phase. This causes more charges to develop around the bubble. Bubble-induced charges are measured as they pass through the sensor. This has the opposite sign as the particle charges in front of the sensor. Signals collected from four sensors radially placed around a bubble are used to reconstruct the charge distribution around the bubble [46, 47]. Since particles move chaotically in a dense-phase bed, back-mixing significantly affects measurement accuracy, and correlation velocity only represents particle motion near the wall [19]. A shielded induction probe has also been used to characterize the electrification of fluidized beds to eliminate particle interference and charge transfer caused by collisions between particles and the probe [57,58]. Non-contacting induction sensors do not disturb flow since they do not directly touch the fluidized material. Since contact charging can reasonably be ignored with non-contacting sensors, it is easier to reconstruct charge distributions from their signals than contacting probes [19]. In contrast, they do not provide adequate local information on non-homogeneous flow systems because particle-wall interactions dominate the signal output rather than particle-particle interactions. A similar sensor array was used by Dong et al [48] to measure the relative charge level in a bubbling bed based on recorded induced currents. While the current amplitude is affected not only by the charges on particles but also by the velocity and concentration of the solid. However, the measured "charge level" only qualitatively represents particle charges without considering the solid's velocity and concentration.

4. TRIBOELECTRIFICATION

Electrostatic phenomena originate from frictional charging, triboelectrification, and contact charging. These phenomena are induced by particle-particle, fluid–particle, and particle–wall contacts and frictions [19, 26]. The process of triboelectric charging or triboelectrification occurs when two materials are brought into contact, and then separated. There have been many debates over triboelectrification mechanisms, including electron transfer, ion transfer, and material transfer [56,59]. Because surface atoms represent a tiny fraction of charge carriers, it is difficult to determine the identity of the charge carriers. [60, 61].

According to Pan et al [62], the most obvious difference between these three media is their ability to carry a unit charge. Table 1 provides this classification.

Table 1. The general difference among electron, ion and [Nano-] material [62].

Tribocharging media	Basic unit	Mass	Unit charge carrying capacity
Electron	Electron	Low [~10^{-31} kg] Medium [~10^{-20}-10^{-27} kg]	1 [Medium; Constant]
Ion	Ion	No consideration for macromolecules/ions	Usually 1-10 [Large; Ions may carry multiple charges]
[Nano-]material	Atom & Ion	Extremely high [>10^{-12} kg]	<<1[small; some atoms carry no charge]

- Electron

The surface work function is a measure of the work or energy required for an electron to be pulled away from a material's surface. This is when electrons are used as a charging medium. As metals have lower work functions than non-metals, they lose electrons more easily when in contact with other materials. Electrons flow from the surface of a material with a lower work function to the surface of a material with a higher work

function when two dissimilar materials are in contact. Dielectric particles extract electrons from neutral metal surfaces when they contact them [62].

- Ion

Due to several similarities in electron transfer and ion transfer, a lot of importance is placed on distinguishing between electron sources and ion sources for charging in triboelectricity. Even though the effective work function can explain the electrification of metal–insulator tribe-pairs, electron transfer between insulator–insulator tribe-pairs is often considered impossible [60]. During ion transfer, ions of one charge polarity may be tightly bound and those of the other charge polarity loosely bound. When tribological contact is initiated, the imbalance of affinity for various ions will lead to the transfer of certain types of ions. This will result in the accumulation of charge on the surface [63]. As ions transfer predominantly at the metal–polymer interface, the metal surface property is relatively trivial, and the charge is believed to be largely derived from protons dissociated from ambient water.

- [Nano-] material

The transfer of material resulting in charging occurs when vigorous rubbing or pressing is applied [64, 65]. For instance, a polymer can exchange material from deeper layers when rubbing with friction [66]. The reason why even identical polymers can be charged by tribo-contacts is that even identical polymers have different compositions at each depth, which explains the same material charge transfer [64]. Further, if dynamic changes happen on surfaces and in tribological environments, material transfer may occur, as materials tend to move toward a lower potential energy state, resulting in potential energy minimum shifts [67, 68].

4.1 Triboelectric series

A triboelectric series is a list of empirically ordered materials. This illustrates how charging occurs when two materials are brought into contact by rubbing, pressing, or friction. Positive charges are associated with materials higher on the list and negative charges are associated with materials lower on the list [69,70]. Figure 7[69] summarizes the triboelectric series. Chowdhoury et al. [71] examined electrostatic charging from particle-particle collisions of aluminum, PTFE, and nylon, finding that the charge gained on all three materials fell into the triboelectric series. Despite the triboelectric series' superior fitness, some contradictory experiments have been published. [43,61, 72, 73].

As a result of fluidizing polyethylene and glass particles with argon, nitrogen, and air in acrylic and steel columns with varying humidity levels, Hou et al. [73] observed that the experimental results were consistent with the triboelectrification series. HDPE particles were negatively charged in an acrylic column, while glass beads were positively charged. Glass beads in the steel column acquired negative charges, against the triboelectric series, or even acquired different polarities in humid environments. Dry and humid gases may affect the glass's position in the triboelectric series in different ways.

Charge transfer and charge separation may be responsible for the triboelectric charging of particles in fluidized beds [24,74]; charge transfer results in similar surface polarities while charge separation results in opposite polarities at the contact interface. Known as bipolar charging, charge separation is the process of polarizing charges between particles of the same material with different sizes [24, 75]. So, regarding this item, the results by Hou et al. may also be due to bipolar charging fine and coarse particles [73].

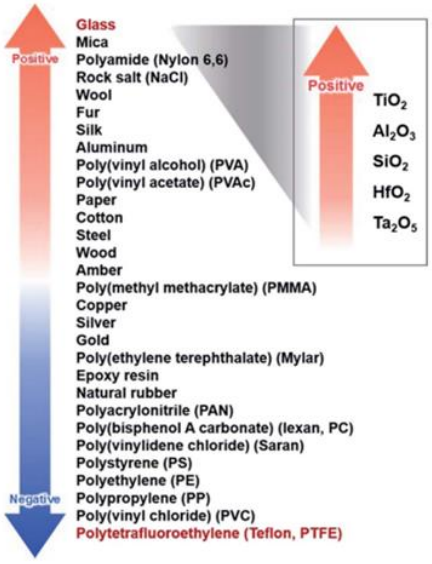

Fig. 7. A conventional triboelectric series and an experimentally determined triboelectric series of oxide dielectric materials [69].

4.2 Triboelectrification Mechanisms

Bipolar charging due to particle-particle contact is believed to be the dominant charge generation mechanism in gas-fluidized beds [5, 76], which is responsible for most electrostatic-related phenomena in fluidized beds such as particle agglomeration and wall fouling [77, 78].

According to a theory [79], particle size depends on work function. This can result in charge species [electrons and ions] being transferred from larger particles with smaller work functions to smaller particles with higher work functions by triboelectric charging. When the wall's work function and that of the particles in the bed differ greatly, charge transfer is high. Once a stagnant particle layer forms on the wall, macro-structures eventually gain their maximum energy [5]. It is crucial to distinguish charge distributions in fluidized beds because particle sizes can vary greatly. It is believed that a wide particle size distribution is a significant factor in polyolefin fluidized bed reactors [36]. Across a fluidized bed, electrostatic field strength and particle polarity are different. As Gajewski et al. [80] measured polypropylene particles' electrification. They found that electrification occurs primarily on the grid, with electrified particles carried to the surface where they dissipate their charge. A study conducted by Ali et al. [31] revealed that tribocharging occurs in fluidized beds of polymer powders. However, induction charging can also take place in fluidized beds of these insulating particles. Results showed that the charge density inside the bed was quite uniform, except for some fine powders being deposited onto the walls in the near-wall region. Wall deposits were found to be positively charged in the dense bed region, and the charge density increased with height above the distributor. The negative polarity of deposits was observed above the bed surface, no deposits were found on the wall where the charge density was zero, and there was a difference in mean volume size and charge polarity between the wall deposit particles below and above the dense bed. Thus, they hypothesized that the wall deposit particles above the dense bed were originally positively charged, but became negatively charged due to the electric fields induced by fluidized charged particles. Fang et al. [81] measured electrostatic charge distribution using a three-dimensional gas-solid fluidized bed of LLDPE. They found that the electric field inside the bed was non-uniform. At the interface between dense and dilute phases, voltage polarity reverses, resulting in a Z-shaped potential profile. In addition, increasing radial distances from the column increases the electrostatic voltage. Regarding the relationship between charge distribution and particle size distribution in fluidized beds, the net charge on small particles determines the polarity at the top of the bed. In contrast, the net charge on large particles determines the electric field at the bottom of the bed. As a result of this study, three special zones were identified: distributor, stagnant, and bed-level zones, the latter two having higher voltages and being more easily disturbed by particle adhesions and even wall sheets. Finally, they claimed that in large vessels, bipolar charging is dominant due to contact between particles. In small vessels, monopolar charging is predominant due to particle and wall interactions.

In two studies, eight ball probes were positioned above and near the wall of a fluidized bed of polyethylene powder [53,54,82]. Those probes always delivered negative currents in the lower dense bed region, but positive currents in the upper and freeboard zones. This confirmed polarity reverses as bed height increases. In Giffin et al.'s work [83], relatively small particles become predominantly positively charged while larger particles become predominantly negatively charged. There was a significant difference between the magnitude of net specific particle charge in each region of the bed. This was with elutriated fines having the largest magnitude, followed by the fines that adhered to the column wall, and finally those in the bulk of the bed. Using a wide range of particle sizes, Sowinski et al. [27] observed bipolar charging in both bubble and turbulent flow regimes. There was A net negative charge in the fines entrained in the column wall and the bed, while the fines attached to the wall and the bed carried a positive charge. In the bubbling regime, the charge-to-mass ratio [q/m] of the entrained fines was significantly higher than in the slugging regime. There was evidence that particles with a particular size range adhered to the column walls with a significantly higher q/m than the other particles in the bed. Furthermore, the flow regime had a large impact on the electrostatic forces generated within the fluidization column [triboelectrification and frictional charging], which controlled particle migration. According to Tiyapiboonchaiya et al. [84] both positive and negative electrical currents were traced throughout the entire bed. Positive current values were observed at the bottom of the bed, while negative current values were observed at the top of the bed. In experimental and theoretical studies, Ji et al. [85] and Chen et al. [86] investigated the effects of particle size distribution on triboelectric charging polarity in beds of identical materials. Smaller particles charged negatively in insulator systems containing similar particle sizes, while larger particles charged positively. Pei et al. [87] studied contact electrification using a DEM–CFD model validated by experimental results. Larger particles achieve a higher equilibrium charge but a lower charge-to-mass ratio than smaller particles. Particles of differing sizes will, however, ultimately have the same surface charge density. Moreover, it was shown that charge is initially generated near the walls and propagates throughout the bed, as a result of particle mixing and particle-particle collisions. Experimentally, charge accumulation eventually reaches an equilibrium state, following an exponential trend. During a series of experiments conducted by Alsmari et al. [88] with fine and coarse particles (glass beads and polyethylene), bipolar charging was observed in all experiments, with fine particles being positively charged and large particles being negatively charged. Experimentally investigating the distribution of charge in fouling particles, Song et al. [32] proposed a mechanism for particle build-up on column walls. Results showed that both positively and negatively charged particles were present in the polyethylene layer built up on the column wall. According to the proposed mechanism, charged particles migrate toward metallic column walls due to electrostatic and image forces. Image forces were attributed to particle/wall contacts. Electrostatic forces could be attributed to the contact between oppositely charged particles within the bed and those fouled on the column wall. While identical materials were used in some experiments, the surfaces of particles of the same material were not truly alike. This is because there is a statistical distribution around the mean value of the materials' properties. Since only a very small number of charged, species are required to produce an electrostatically charged surface, these statistical variations can significantly affect charge transfer. For example, a highly charged surface has only one excess species per 105 surface atoms [89]. Lowell and Truscott [90] proposed that triboelectric charging between identical surfaces may be explained by asymmetric contact. According to this theory, charge transfer species are trapped in high-energy states on out-of-equilibrium surfaces.

Overall, the discrepancies among the studies can be attributed to the different column materials and dimensions. In addition, the type and size of fluidized particles, relative humidity, which will be discussed in other sections, and bed height. It is noticeable that the influence of particle size on work function is negligible for particles larger than 1 μm [89].

5. EFFECTS OF ELECTROSTATICS ON HYDRODYNAMICS

Numerical and experimental studies have demonstrated that electrostatic charges can affect fluidized beds hydrodynamics. In this way, gas bubble characteristics and entrainment are two key parameters to consider. Moreover, electrostatic charges can change the forces on particles [48,91,92], thereby inducing particle-wall adhesion, inter-particle cohesion, and agglomeration [4, 9,93], which can further affect electrostatic phenomena in the bed.

5.1 Bubble characteristics

The performance of a fluidized bed is related to particle motion, while gas-solid contact is primarily governed by its bubble characteristics. As a result, the bubble phenomenon plays a particularly critical role in multiphase flow structures [94]. Bubbles formed in a bubbling fluidized bed are responsible for proper solid

circulation, and gas-solid contact area, which determines heat and mass transfer within the reactor. Bubble properties can be used to describe bubble behavior, including bubble diameters, bubble rise velocities, and bubble frequencies. Bubble size in fluidized beds is affected by several factors, including gas distribution, particle size distribution, bed geometry, superficial gas velocities, and bed height. As soon as the bubble size equals the bed diameter, the bed changes from bubbling to slugging. By increasing bubble size, the bubble rise velocity increases, which reduces the contact time between gas and solids within the reactor [16, 95-100]. It is necessary to study the effects of electrostatic charge on fluidization hydrodynamics in three cases to accurately investigate the effects of electrostatic charge on bubble behavior and regime transition velocities: an uncharged bed reflecting the minimal electrostatic influence, a bed of pre-charged particles illustrating the effect of the initial charge of particles, and finally a bed of charged particles demonstrating the fluidization process as a whole. In gas-solid fluidized beds, bubbles are formed at the distributor plate, grow and rise to the bed surface, and burst. Figure 8 shows bubbles in the emulsion phase.

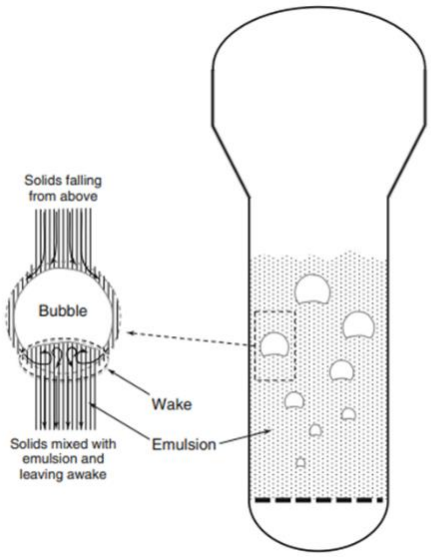

Fig. 8. A schematic of gas and solid flows in a bubbling regime [6].

Pressure fluctuations are commonly used to study the dynamics of fluidized beds [15,101,102]. The movement of a single bubble injected from an orifice into the bed has been considered a suitable method to understand pressure fluctuations [103-106]. Pressure waves in a gas–solid fluidized bed can be dynamic or kinematic, with dynamic waves traveling fast and kinematic waves traveling slowly [105,107,108]. Dynamic pressure waves travel upward and downward at high speeds. Fast upward waves result from the formation and coalescence of bubbles, whereas fast downward waves result from bubble eruption. Kinematic waves account for local phenomena such as gas bubbles rising and agglomerates and clusters moving. [97]

As reported by Bi et al. [104], pressure waves travel upwards and downwards, and their propagation is determined by particle interaction. A study by Schaaf et al. [105] attributes the measured pressure fluctuations to fast and slow pressure waves. Upward-moving compression waves (> 10 m/s) are linearly dependent on the distance to the bed surface and originate from gas bubble formation and gas bubble coalescence. A downward-moving compression wave is induced by gas bubble eruptions at the fluidized bed surface, bubble coalescence, and changes in bed voidage. It is independent of the distance from the bed surface. Rising gas bubbles cause pressure waves with propagation velocities less than 2 m/s. These waves propagate only upwards, with an amplitude proportional to the bubble size. Pressure waves are generally generated by variations in gas or particle velocity and voids in the bed. Bi and Chen [109] measured pressure fluctuations and showed that the maximum amplitude increased with increasing the superficial gas velocity and static bed height for relatively shallow beds. This was insensitive to static bed height increases in relatively deep beds. Bi [110] indicates that pressure fluctuations are the result of multiple sources, including local bubble-induced fluctuations, global bed oscillations, and propagating pressure waves originating at the surface of the bed or distributor plate. Using ultra-fast Magnetic Resonance Imaging (MRI), Muller et al. [111] found that the frequency of bubble eruptions from the top of the bed matched the frequency of pressure fluctuations just above the distributor. Pressure

fluctuations were attributed to bubble passage and eruption at the top of a bed. Based on a 3D model with computational fluid dynamics, Boyce et al. [112] investigated the origin of pressure fluctuations in bubbling and slugging fluidized beds and found that their results were completely consistent with Muller's.

Manafi et al. [5] investigated pressure fluctuations in beds of glass beads and polyethylene particles. Neither hydrodynamic structures nor the transition velocity to the turbulent regime are affected by bipolar charging in a bed of particles with a narrow size distribution. Near the wall, the voidage decreases, causing bubbles to rise from the middle of the column and coalesce faster, leading to larger bubbles. Nimvari et al. [97] studied the source of pressure fluctuations and behavior of a single bubble in a two-dimensional gas–solid fluidized bed of two types of Geldart group B particles, glass beads, and sand. According to the results, bubble formation maximum amplitude was independent of bubble diameter. Although it depends on particle density, injection velocity, and distance from the bed surface. On the other hand, bubble eruptions had maximum pressure fluctuation related to bubble diameter, density, and particle size. Based on the study results, pressure fluctuations are caused by changes in dense phase voidage, bed voidage, and particle movement during bubble eruptions. Gas-fluidized beds are characterized by density fluctuations, caused by bubbles, which form spontaneously and grow in size as they rise through the bed [103]. To characterize the electrostatic charges Yao et al. [113] conducted experiments on polyethylene resin in freely bubbling fluidized beds. They found that when voltage signals are amplified, bubble size, rise velocity, and charge density around the bubble will increase. When the standard deviation of differential pressure fluctuations decreases, the charge density in the vicinity of bubbles will likely decrease as well as the bubble size.

Jalalinejad et al. [114] modeled the injection of single bubbles into a fluidized bed of charged and uncharged particles by the Two-Fluid Model (TFM). The simulation predicted bubble elongation in the flow direction. Bubble elongation is primarily due to the electric field varying only horizontally. The electric field causes a denser bed close to the outer walls, leading to more gas flow near the column axis. Bubbles rose faster than in the non-charged case, which was compatible with Gidaspow et al. [58] and Rahman and Campbell [82] for uncharged particles. Hassani et al. [115] simulated the electrostatic effect in unipolar and bipolar-charged beds via a combination of a 3D discrete element method (DEM) and a coupled computational fluid dynamics (CFD) model. The results showed that as the electrical charge increased, bubbles shrank, solids diffusivity declined, and the void fraction decreased. Voidage distribution results in fewer bubbles and more homogeneity in the bed and solids circulation. It was also discovered that chains of connected particles are formed when opposite charges are introduced into the bed. In addition, bubble shape and voidage distribution approach those of neutral beds as well. According to Dong et al. [48], increasing the level of electrification of particles resulted in greater velocity, bubble sizes decreased, and bed surface fluctuation weakened, so fluidization quality declined. The electrostatic force causes fluctuations in particle motion and distribution, while particles have a single polarity, which makes repulsion the dominant force. The repulsion force among charged particles and the attraction between particles and walls augment wall sheeting. Jalalinejad et al. [116] simulated bubble injection into a fluidized bed in vertical and horizontal alignments. Comparison in vertical alignment shows different bubble coalescence behavior, with significant asymmetry in the charged case, leading to a larger bubble. For bubbles in horizontal alignment, the results were similar to those of previous modeling [114]. In completing this simulation, Jalailnejad et al. [117] experimentally studied this issue by injecting bubbles into a two-dimensional fluidized bed of charged particles. According to the results, bubble shape and stability are influenced by charge density distribution. As charges accumulate in a fluidized bed, bubbles grow smaller and split more, which influences bubble rise velocity. The non-uniform distribution of charge density may explain the differences between simulation and experiment.

Tan [94] figured out that in a highly charged bed, the length of the bubble in the y-axis direction to the length in the x-axis direction gradually decreases as the rising height increases. Tan also implemented a simulation using the Two-Fluid Model (TFM). According to numerical results, electrostatic force has a negligible effect on particle motion around a bubble in the y-direction but is prominent in the x-direction. Due to electrostatic force, bubbles elongate and particles in the middle region of the fluidized bed tend to move around. This results in more gas accumulating from the emulsion phase to the bubble region. Manafi et al. [118] investigated the bubble behavior of polyethylene particles (uncharged, pre-charged, and bed-charged). The bulk electrostatic charge of a gas increases as the gas velocity increases. At high gas velocities, the repulsive force among highly charged particles overcomes the particle-wall effect on bubble formation and reduces bubble size to less than in uncharged experiments. In the bed, particle accumulation has two effects on hydrodynamics: first, it accelerates bubble growth via bubble coalescence at low gas velocities, and second, it limits bubble growth and decreases the transition velocity to the turbulent regime to a value lower than the transition velocity for pre-charged particles. In a subsequent study, they investigated Geldart B particles. As

the adhesion layer to the wall prevents particle-wall contacts, particle electrostatic charge accumulation would not reach the maximum electrostatic charge accumulation predicted by theoretical equations [119]. During fluidization, this stagnant layer reduces the fluidized portion of the bed, reducing the pressure drop of bed-charged particles. In experiments, it was also found that particle-specific charge increases with increases in excess gas velocity, U-U_{mf}. Repulsive electrostatic forces among charged particles increase bed voidage, which increases gas velocity. To evaluate the electrostatic force along the bed, a theoretical model was developed. This confirmed that the bed voidage rises at the minimum fluidization velocity. Transition velocities from bubbling to turbulent fluidization and the maximum standard deviation decrease by raising the charge density. Moreover, as the bed voidage increases, bubble size decreases, which lowers the turbulent fluidization transition velocity. A recent study using computational particle fluid dynamic (CPFD) simulations revealed that bubble diameter, bubble frequency, and bubble rise velocity are directly dependent on superficial gas velocity. Increasing superficial gas velocities up to 4.2 U_{mf} results in larger bubble diameters. The bubble rise velocity is not linear, and it grows while moving from the lower region to the bed surface. This is due to an increase in superficial gas velocity. Furthermore, the bubble frequency increases with an increase in superficial gas velocity up to 2.5 U_{mf} and decreases with a further increase in gas velocity [16]. Gas bubble characteristics including bubble size, rise velocity, and frequency are of paramount importance for a specific application. The discrepancies in electrostatic impact in these studies may be due to different wall effects on bubble properties in 2D and 3D columns, measurements, and material properties that have been tested.

5.2 Entrainment

In a gas-solid fluidized bed, entrainment or fine particle carry-over can choke downstream equipment. A cyclone and bag filter can capture entrained particles. Recovery systems require an entrainment flux to determine effective parameters. Correspondence has been defined for particle entrainment in beds. A substantial discrepancy between experimental data has been observed due to the inappropriate use of empirical constants. Chew et al. [120] provided a comprehensive review of the available correlations for entrainment in the gas-solid fluidized bed. Mehrani et al. [40] studied the effects of adding various fine particles to gas–solid fluidized beds on electrostatic charge changes for a range of relative humidity. They found that the entrained fine particles from the column were charged with opposite charges by the large bed particles. Charge quantity depends on particle size, physical and chemical properties, and the moisture content of the gas in the bed. Moughrabiah et al. [53] found that fine particles carried bed charges. Sowinski et al. [27] investigated the electrostatic charge distribution of polyethylene particles in bubbling and slugging flow regimes. Results indicated that the charge-to-mass ratio of the entrained fine particles in the bubbling flow regime was remarkably higher than in the slugging regime. Alsmari et al. [88] examined the entrainment of a mixture of fines, such as glass beads, polyethylene, and alumina, and coarse particles, including glass beads or polyethylene. The results indicated that particle entrainment flux grew as fine concentration increased. This can be attributed to the increase in the weight fraction of particles in the bed and inter-particle adhesion forces. In addition, fine concentration had a negligible effect on fine charge densities. Increasing coarse particle density, increasing electrification, and decreasing the entrainment flux of particles can result in more energetic collisions between particles. A study by Fotovat [121] examined the effects of entrainment on conductive and non-conductive fine powders. They showed that the entrainment rate of dielectric fine particles was lower than conductive fines, possibly due to the increase in electrostatic inter-particle forces for dielectric particles. As a result of the distribution of non-uniform electrical charges and the attractive forces among these particles, agglomeration occurs, which reduces entrainment because of agglomeration. Also, the repulsive electrostatic forces between conductive particles enhance their entrainment.

6. EFFECT OF HYDRODYNAMICS ON ELECTROSTATICS

It is proved that the hydrodynamic behavior of fluidized beds has a direct impact on the net electrostatic charge produced in a fluidized bed. Gas velocity, operating temperature, and pressure, fluidizing particles in terms of size and material properties, relative humidity, and fluidization time are factors that should be taken into consideration while hydrodynamic effect is being considered.

6.1 Effect of gas velocity

Increasing the fluidizing gas velocity will cause the bed to enter various flow regimes, such as bubbling, slugging, and turbulent flow. This will affect electrification.

In the bubbling regime, electrification increases with increasing superficial gas velocity in fluidized beds [52-54,73,122-126]. As bubble size and rise velocity increase, the bed circulation rate increases, resulting in

enhanced particle movement and particle-particle contact [124, 127,128]. Slugging fluidization, however, limits this trend by creating slugs when bubbles grow too wide and reducing particle movement [124]. Sowinski et al. [27, 26] measured the mass and charge of the particle layer fouled on the column wall after one-hour fluidization. In the bubbling flow regime, wall coating was greater. During bubbling flow, the amount of wall layer coating and the layer net charge-to-mass ratio increased as the gas velocity increased, while at the onset of slugging and beyond, the net charge density plateaued. It can be concluded from the plateau in the results that the particle's charge was lower in the slugging flow regime. Fotovat et al. [75] pointed out that in the slugging flow regime, where tribo-charging is dominated by particle-wall interactions rather than particle-particle interactions, enhancing the superficial gas velocity results in no change or decrease in the bed electrical potential and net charge density, which is associated with a less polymer particle coating on the walls than when bubbling or turbulent fluidized. Song et al. [32] studied the effect of gas velocity on electrostatic charge generation in gas-solid fluidized beds at a pressure of 2600 kPa [abs] with fluidized gas velocities of 1.5, 3, and 5 times U_{mf} (pre-turbulent regime) and 7.5 times U_{mf} (turbulent regime). As the gas velocity increased and the turbulent flow regime transitioned, particle-wall contacts improved, resulting in an augmentation of wall fouling, which indicates that electrostatic charges were more generated in the bed. In the turbulent flow regime (7.5 U_{mf}), fouling was approximately five times greater than in the bubbling flow regime (1.5 U_{mf}). A study by Giffin et al. [83] examined electrostatic charge generation in a polyethylene bed under bubbling and slugging flow regimes. The bubbling flow regime resulted in longer and thinner particle layers forming on the column wall. In contrast, the slugging flow regime resulted in shorter and thicker particle layers.

6.2 Effect of Particle size

Particle size distribution causes different fluidization behaviors, as dominating mechanisms and forces are affected [4,43]. Fine particles are difficult to fluidize, while large particles induce the formation of very large bubbles known as slugs, which result in poor-quality fluidization [129]. The effect of particle size on the rate of charge generation and dissipation in gas–solid fluidized beds has been the aim of many experiments presented in a couple of papers. Boland and Geldart [130], and Guardiola et al. [124] concluded that increasing particle size increases bed potential, since particle–particle contacts grow and bed voidages decrease. Wolny and Opali´nski [45] conducted a series of experiments on a bed of polystyrene to test the effects of fine particles. There were 8-12 orders of magnitude reduction in electrostatic forces in the bed containing fines compared to the bed containing pure polystyrene beads. Due to the fine particles, the contact surface area in the bed was reduced by 4–6 orders of magnitude. Yu et al. [131] tested adding different sizes of LLDPE particles to the same coarse ones. Electrostatic behavior in the fluidized bed was strongly affected by injecting small particles into the fluidized bed. Moughrabiah et al. [51] added glass beads fines to a fluidized bed of relatively large glass beads [574 µm]. With higher fine proportions, electrification decreased, charge fluctuations decreased, and fluidization became smoother. Small particles alter particle contact modes and electrostatic charge generation, transfer, and neutralization.

Particle properties and experimental conditions affect different results. According to Kato and Li [132], the elutriation rate constant of group A particles is affected by particle properties, operating conditions, and gas velocity. The elutriation rate constant of group C particles decreases with increases in the mean diameter of bed particles (a combination of several groups) or with decreases in the particle size of group C particles. In similar works, Nakazato et al. [133] reported that the elutriation rate of group A and C particles is aff-ected not only by the properties of the group A particles but also by the weight fraction and size of the group C powder in the bed. This phenomenon was attributed to the bridging eff-ects associated with cohesive fine powders. Baeyens et al. [134] found different results because cohesive powders have different sizes. Alsmari et al. [88] investigated the effects of coarse particle average size on cumulative charge and entrainment flux in fluidized beds containing Geldart group A and B particles. As the size of the coarse particles decreased, the electrostatic charges inside the fluidized bed increased slightly, but the entrainment flux decreased. Sowinski et al. [36] studied the effect of particle size of sieved polyethylene resin on electrostatic charge generation and reactor wall fouling. This was done in both bubbling and slugging flow regimes. Smaller particles were found to have a higher charge and cause more fouling of the reactor walls. Mehrani et al. [135] evaluated particle sizes using a polyethylene fluidizing bed (smaller than 400 µm). It appears that small particles generate substantial net-specific charges. The magnitude fraction of smaller-sized particles plays a critical role in particle electrostatic charging and adhesion to the column wall. As the fraction of small particles in the mixture increased, fouling also increased, with the coating becoming dominated by smaller particles. They concluded that the number of small particles plays a significant role in bed electrification. In addition, the extent of particles coating the reactor wall is due to electrostatics [36,135].

6.3 Material properties

Under completely similar operating conditions, the magnitude of the cumulative charge is likely to be different as a result of material properties. Hendrickson [4] pointed out that polymers with a higher molecular weight are more likely to accumulate electrostatic charges than those with a lower molecular weight. The mechanism through which charges are formed in polyethylene depends on its structure, according to Aida et al. [136]. Branching, co-monomer type, co-monomer incorporation, and polymer crystallinity influence charge formation. Polyethylene with straight chains or short chain branching, such as HDPE, accumulated less charge than lower crystallinity polymers, such as LDPE, because the high crystallinity of HDPE (~ 60–80%) decreased the ease of ionization or di-electrophoresis of impurities. Matsusaka et al. [137] acknowledged that particle material influences bipolar charge distribution. Moughrabiah et al. [51] conducted a series of experiments on three types of LDPE, a defined grade with similar particle sizes but produced with differing catalysts. At specific locations, polymer particles had the opposite polarity. Meanwhile, the degree of electrification in the lower bed and near the wall was insensitive to fluidized particle composition. In these regions, there may be fewer bubbles. In addition, electrostatics were investigated under completely similar operating conditions in fluidized glass bead beds. For glass bead particles (density: 2500kg/m3), the cumulative charge was approximately three orders of magnitude greater than for HDPE particles (density: 965kg/m3). It is likely due to glass beads having higher electrical conductivity than polyethylene, facilitating more charge transfer. As a final step, particle density was examined about electrification levels in beds of LLDPE and HDPE particles. A comparison revealed that the net cumulative charge in polyethylene systems of different densities and similar mean particle sizes was similar. This means that it is likely to be insensitive to differences in particle density [51].

6.4 Effect of operating pressure

The operating pressure affects the hydrodynamics of gas-solid fluidized beds, resulting in electrostatic charges. In a polyethylene fluidized bed, Song et al. [138] investigated the effect of operating pressure between atmospheric pressure and 2600 kPa. By increasing the operating pressure, the mass percentage of particles collected at the wall regions as a result of wall fouling increased (Figure 9). Moughrabiah et al. [53] and Song et al. [30] reported similar results. At atmospheric conditions, larger gas bubbles caused more contact between the particles and the fluidized bed wall. Consequently, particles coating the wall were primarily negatively charged due to a higher degree of image force formation. During pressurization, smaller gas bubbles formed. As a result, electrostatic forces between negatively charged wall particles and positively charged bulk particles increased. It also attracted the inner negatively charged layer to the column wall by positively charged particles forming the outer layer (Figure 10).

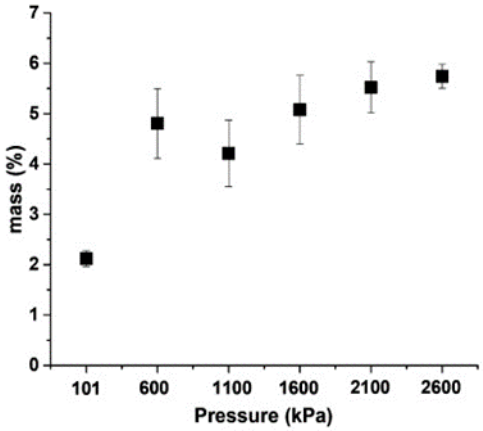

Fig. 9. Mass percentage of particles collected on the wall [138].

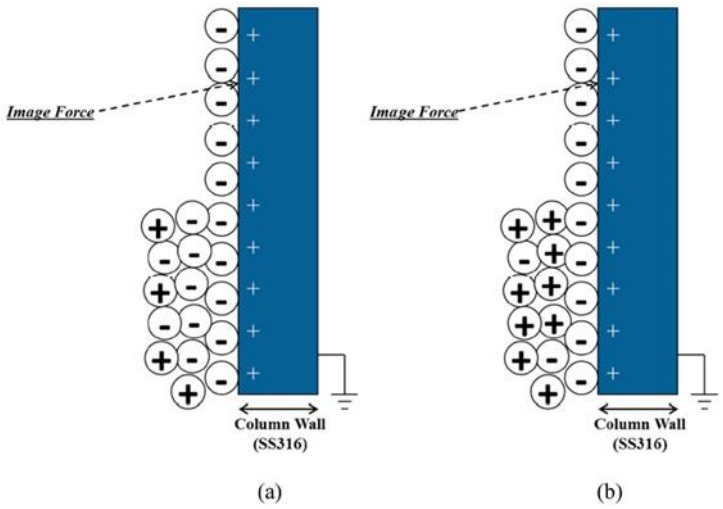

Fig. 10. The mechanism of fluidized bed wall coating formation at [a] atmospheric conditions, [b] under higher pressures [138].

6.5 Effect of temperature

In fluidized beds, temperature plays a significant role in determining particle electrostatic charge. Nimvari et al. [139] studied the effects of 24 to 58 °C temperatures and two pressures of 101 and 2600 kPa in a bed of polyethylene resins. A decrease in the net specific charge of bulk particles (q/m) was observed by decreasing the amount of charge transfer between particles and particle-wall collisions as temperature increased. This resulted in lower electrostatic charge generation within the bed, and a reduction in fouling on the column wall at both pressures (figure 11). Alsmari et al. [123] also reported a similar change in glass beads' electrostatic charges when the temperature increased from 20 to 75°C. Moughrabiah et al. [53] studied the effects of temperature on electrification in a fluidized bed of glass beads and different grades of polyethylene resins. By increasing the temperature (up to 75 °C), bed fluidization improved and electrostatic charges decreased.

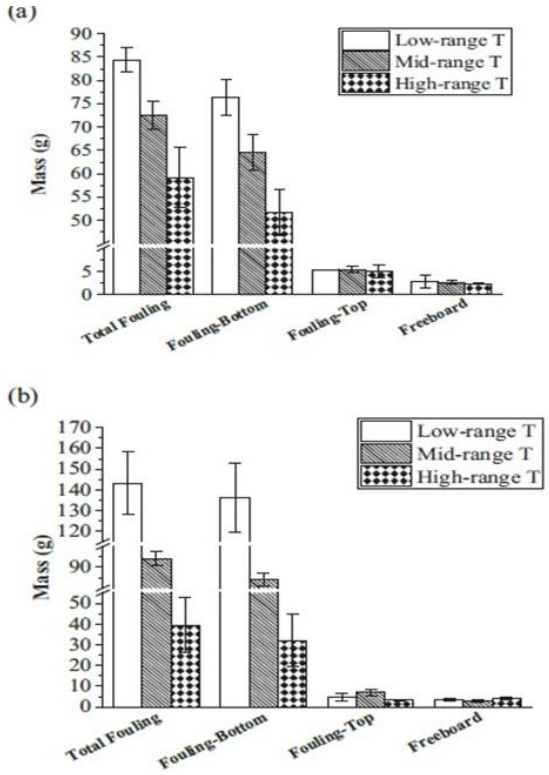

Fig. 11. The amount of wall fouling and its distribution within the column at different operating temperatures. (a) 101 kPa and (b) 2600 kPa [139].

6.6 Effect of fluidization time

Fluidization time affects the electrostatic charge and particle size distribution in gas-solid beds due to frequent contact, chemical reactions, fines entrainment, and particle agglomeration [51,88,115,122].

Giffin et al. [83] investigated the charging effect in both the bubbling and slugging flow regimes for polyethylene particles in three regions of the fluidized bed: elutriated fines, bulk particles inside the bed, and particles adhered to the column wall. As fluidization time increased, particle masses collected in the bulk region decreased and those adhered to the column wall increased during bubbling flow velocities. In the regime of slugging flow, the number of particles in each region was not affected by fluidization time. For all gas velocities and bulk particle sizes, charge saturation was achieved after 60 minutes of fluidization. Charge saturation of fines in a slugging flow occurred shortly after fluidization commenced. In contrast, extended fluidization times were required for entrained fines in a bubbling flow. It was also found that the mean particle diameter for each measurement region was not impacted by fluidization time. This was for any of the gas velocities tested. As fluidization time increased for these velocities in the bubbling regime, bed hydrodynamics affected particle–wall fouling. A particle layer continued to develop on the inner column wall as fluidization time increased. Conversely, the slugging flow had a relatively small impact on particle layer growth. Manafi et al. [5] evaluated the effects of fluidization time on charge transfer and bipolar charging [charge separation] using glass beads and polyethylene particles in a glass column. Further fluidization results in an increase in particle electrostatic charge. The repulsive electrostatic force between particles and the void fraction in the emulsion phase increases with time as electrostatic charges with the same polarity increase in bulk particles. Based on Revel et al. [92], increasing fluidization times causes electrostatic charge to rise and reach equilibrium.

6.7 Effect of Relative Humidity

The effect of relative humidity [RH] on electrostatics has been proven in several studies. Results show that relative humidity can be used to control electrostatic charging in a fluidized bed like polyolefin reactors under BP (British Petroleum) license.

Ciborowski and Wlodarski [126] demonstrated that fluidization air humidity affects minimum fluidization velocities. As humidity decreased, minimum fluidization velocity increased. This is indicative of stronger

electrostatic forces, causing a rapid increase in potential followed by a rapid decrease. Tardos and Pfeffer [140] fluidized porcelain particles with air while the air humidity was 20-60%. RH from about 24% to 36% resulted in a 2–5 times decrease in measured particle charge. Wolny and Kazmierczak [141] indicated that polystyrene particles in a fluidized bed are probably heteropolar. By increasing fluidized air humidity, fines could be removed from the bed more easily. As explained by Park et al. [125] increasing the humidity reduced the electrostatic charge accumulation by increasing the surface conductivity, which enhanced charge dissipation. Mehrani et al. [40] investigate the effects of relative humidities on the electrostatic behavior of different fines (Larostat 519 antistatic agent, glass beads, silver-coated glass bead, catalyst, and silica particles). They found that, when there is no moisture, due to contact of fines with polyethylene particles, they become positively charged. However, when exposed to these particles with higher moisture content, they help to dissipate bed charges by becoming more conductive due to the presence of water molecules and becoming negatively charged. Moreover, the molecules of water can react with silica and catalysts and change their chemical and physical properties.

Guardiola et al. [124] admitted that the effect of relative humidity is complex and depends on the type of fluidization regime. Chen et al. [142], showed that an increase in relative humidity at RH < 50% resulted in a significant decrease in specific charges. The effect of relative humidity became insignificant beyond 50% relative humidity. Giffin et al. [143] found that relative humidity only affected wall fouling in the bubbling flow regime, where the particle layer on the wall was reduced at 60% and 80% relative humidity. In the slugging flow regime for those particles that adhered to the column wall a decline in particle net charge-to-mass ratio was obtained only at high humidity of 80%. In both flow regimes, other variations in charge and charge-to-mass ratio were observed but did not follow gas relative humidity trends. Németh et al. [144] conducted charging experiments in a range of humidity on several polymers. Figure 12 depicts that each polymer showed different behaviors, attributed to adsorption or swollen layers with increasing atmospheric humidity.

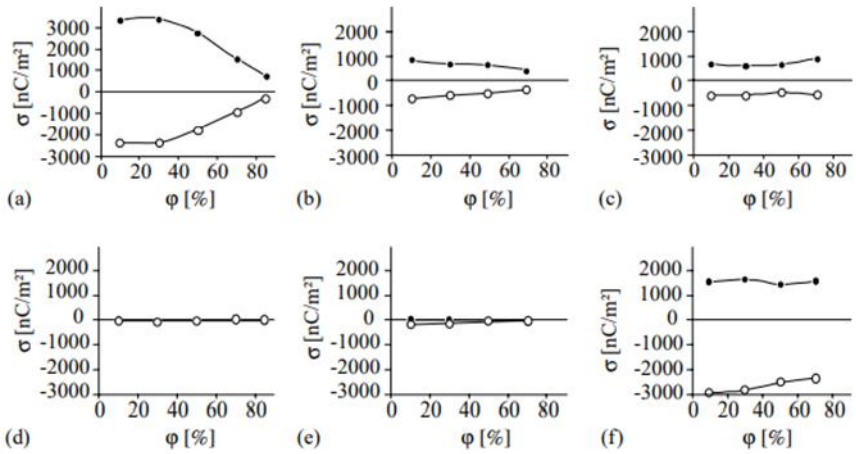

Fig. 12. Surface charge densities [σ] of several polymers in dependence on the relative humidity [ϕ]. Polyamid-12 [a]; Poly [methyl methacrylate] [b]; Poly [ethylene terephthalate] [c]; Polystyrene [d]; Polyethylene [e]; PVC Poly[vinyl chloride] [f]; ● positive charges, ○ negative charges[144].

Nomura et al. [145] investigated the effect of relative humidity on powder tribo-charge in the humidity range of 10-90%. In response to increasing humidity, the saturated specific tribo-charge of the powder decreased. Sharma et al. [146] showed that with increasing relative humidity, the charge-to-mass ratio [q/m] and the surface resistivity of polyethylene powder declined. Fotovat et al. [147] showed that the charge density of fines decreased for dielectric particles and increased for conductive particles with increasing relative humidity [5%-35%]. Hou et al. [73] studied the effect of relative humidity on polyethylene [HDPE] and glass beads [GBs] particles fluidized by different gases in acrylic and steel columns. A maximum charge density was observed at an intermediate humidity level in a steel column, whereas the charge acquired by HDPE particles rose with humidity in an acrylic column. A higher humidity level increases the availability of H+ and OH- ions in the water adlayer, which leads to an increase in particle charge levels. In contrast, water in the

adlayer causes charge relaxation between HDPE particles and a conducting wall. This gives rise to the maximum at intermediate humidity in the steel column. The polarity of GBs changed from negative to positive when the humidity in the steel column increased. The acrylic column followed a similar trend to HDPE in the steel column. Schella et al [148] studied the effect of humidity on the charge accumulation of polymer particles at humidity levels of 5 % to 100 % RH. They found that polymer particles become highly charged at low humidity levels (< 30% RH), but acquire almost no charge at humidity levels above 80 % RH. Kolehmainen et al. [149] reported that the total charge in the system decreased with increasing humidity and was close to zero when humidity reached 60% RH. When humidity values were less than 30% RH there was no large change in the total charge. Similar qualitative behavior was also seen in the results of Schella et al. [148].

According to Sippola et al. [150], the magnitude of the average particle charge was adjusted by changing the relative humidity (0–60 % RH) while keeping other parameters constant. Dry conditions result in particles acquiring a very strong positive net charge. As shown in Figure 13, they tend to charge negatively when relative humidity exceeds 30%. A humidity-dependent polarity reversal was observed, similar to the result of Mehrani et al. [40] for fines entrained from a fluidized bed of polyethylene particles.

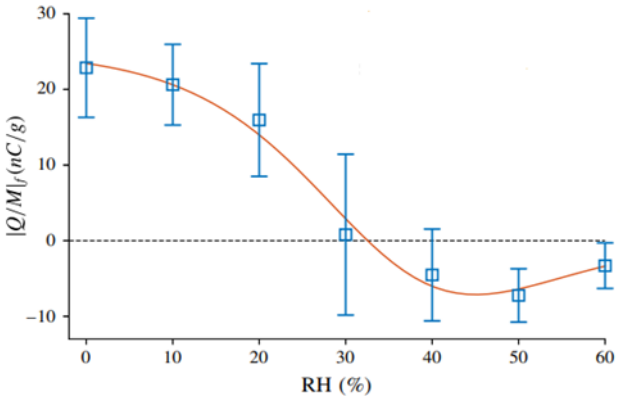

Fig. 13. Final charge-to-mass ratio as a function of relative humidity [150].

Cruise et al. [151] investigated the effect of relative humidity on a range of diameter spherical PTFE particles triboelectrically charged in a stainless-steel column. They admitted that relative humidity affects particle size. From 40% to 60% relative humidity, the saturation charge on the 1.59 mm particle decreases significantly. In contrast, the charge on the 3.18- and 4.76-mm particles experiences a moderate decreasing trend from 50% to 60% relative humidity. The saturation charge of the largest 12.7 mm particle is not affected by relative humidity in the range considered. Of course, increasing the gas humidity in a polymerization reactor is not an option in most cases because the catalysts are typically moisture-sensitive. However, these observations reinforce the efficacy of antistatic agents.

7. CONTROL OF ELECTROSTATIC CHARGE

Electrostatic charge generation in fluidized beds must be controlled to prevent problems such as agglomeration, wall fouling, reduction of product quality, and unscheduled shutdowns [24]. Among the methods used to control electrostatic charge in fluidized beds, there are three main categories: charge generation rate reduction, charge dissipation rate enhancement, and charge neutralization [4]. When working with an electrostatic charge control strategy, many factors need to be taken into account. These factors include reactor operating conditions, reactor design parameters, catalyst type, etc. In the following sections, we discuss practical methods for controlling electrostatic charges.

7.1 Effect of antistatic

An electrostatic charge can be generated in a fluidized bed when catalyst particles come into contact with the reactor wall and polymer particles. They can also charge through pneumatic transport during injection and recirculate within the recycling line [152]. Adding antistatic agents to increase surface conductivity is the most successful method for dissipating electrostatic charges in industrial-scale fluidized bed polymerization reactors [24].

Antistatic agents being used mainly include [4,155]:
· Ethoxylated fatty acid amines (Atmer 163, AS 990).
. Aluminum Distearate
. Calcium and Zinc Stearate
· Quaternary ammonium salts and chromium-containing compounds (Stadis 450).
· C12–C22 fatty acid soaps of alkali or alkaline earth metals.
· Salts of sulfonic acid esters.
· Esters of polyethylene glycol with fatty acids.
· Polyoxyethylene alkyl ethers.

An antistatic layer was applied to the inside wall of a fluidized bed by Mihan et al. [153], which consisted mostly of poly-α-olefin and non-volatile antistatics. In a polyethylene reactor, Moughrabiah et al. [51] studied Larostat 519 as an antistatic agent. They showed that the degree of electrification decreased by increasing the proportion of Larostat 519 from 0.0 to 0.5 wt%. However, it increased when the proportion reached 1.5 wt% because of the agglomeration of Larostat particles due to adsorbing water. He et al. [154] also used Larostat 519 in the proportion of 0.1wt% and observed that the wall fouling was significantly reduced. In another study, the effectiveness of Larostat 264A was investigated by adding 0.5 wt% of this anti-static agent to the airNorpar15-HDPE. the electrostatic level was reduced very quickly by 82.9 % and within one hour the electrostatics completely is vanished from the system [165].

Prostatic agents are used to control wall fouling in polyethylene reactors when introduced as positive charges [e.g., MgO, ZnO, Al_2O_3, and CuO] or negative charges [e.g., V_2O_5, SiO_2, TiO_2, and Fe_2O_3] when added to the bed [43,155]. Taghavivand et al. [72] by applying silica powder found that injection of silica in a dose of 1000 ppm has a noticeable impact on wall fouling. This is because it reduces the bulk particles' charge magnitude and lowers the repulsion forces between them. It also lowers the attractive electrostatic forces of particles on the wall and in the bulk. Wang et al. [9] used metal oxides [TiO_2, Al_2O_3, MgO, ZnO, and Fe_2O_3] as charge-inducing agents in a gas-solid fluidized bed with LLDPE particles. An appropriate quantity of metal oxide at 0.5wt% reduced the electrostatic level in a fluidized bed.

7.2. Charge elimination devices

Electrostatics can be controlled by adding fine particles, increasing relative humidity, manipulating temperature and pressure, and adding antistatic agents, as described in the previous sections. It should be noted, however, that the methods of charge reduction mentioned above are not always applicable to industrial fluidized bed reactor systems. In polyolefin fluidized bed reactors, the particle and reactor wall materials are fixed. A very limited range of operating conditions exists, such as gas velocity, temperature, and pressure. In addition, catalysts are poisoned by small amounts of water and oxygen. Because of this, either reducing the generation of electrostatic charge or accelerating its dissipation is difficult to accomplish. So, ion injection technology can be applied in some cases.

Taillet [156] applied the supersonic injection of electric charges for the elimination of electrostatic charge. By injecting electric charges into the fluidized bulk, a neutral cloud of ions is released. In this process, the cloud neutralizes particles with opposite polarities. Another study by Taillet [157] showed that removing static charges by plasma is impossible when the distance between two particles in contact by plasma is less than the Debye radius. Plasmas have a characteristic length called the screening distance λ_D, also known as the Debye radius or Debye length. When electric charges are located at a distance smaller than this, they interfere with one another. Revel et al. [92] used a supersonic injector to produce a neutral cloud of ions for the elimination of static electricity in polyethylene in a fluidized bed. As a result, the ions emitted from the eliminator were unable to penetrate the bulk of particles, leading to the elimination of static electricity. Kachi et al. [158] investigate the effect of AC Corona discharge from a wire-type electrode on the neutralization efficiency of polyethylene granules. A higher frequency of high voltage improved neutralization efficiency. Dong et al. [159] studied the neutralization of electrostatic charge in a gas-solid fluidized bed by a Corona charge eliminator that includes a needle electrode and a current power supply. Charge neutralization efficiency increases with increasing superficial gas velocity, which has a significant influence on charging processes.

8. THE EFFECT OF CATALYST TYPE

By continuously injecting and recirculating catalyst particles through the polyethylene gas-solid fluidized bed reactor, polyethylene particles are formed through the polymerization reaction [152]. Different catalysts have been used for polyethylene reactions, for example, Ziegler−Natta catalysts, chromium-based catalysts [e.g., Phillips type], and metallocene catalysts. It is important to study the effects of catalyst type on charge

generation in gas-solid fluidized bed reactors. Hendrickson [4] says chrome catalysts are not prone to electrostatic charging. Vanadium and Ziegler-Natta catalysts also create negative charges in gas-phase fluidized bed reactors. Sowinski et al. [152] investigated the effects of a metallocene catalyst and its silica support on electrostatic charging in a polyethylene fluidized bed reactor. Catalysts and supports have a negative specific charge, which attracts positively charged polyethylene particles to the wall region. This leads to wall fouling. Taghavivand et al. [72] examined the effects of amorphous silica catalyst support on charge generation and wall fouling in polyethylene fluidized bed reactors. In the bulk of the bed, the silica powder produced a negative charge that neutralized the positive charge of the polyethylene particles. This decreased the net positive charge in the bulk. As a result, wall fouling is reduced. Moreover, catalyst injection into polymerization reactors via a tube, pneumatically or even as a mixture of grease, oil, and catalyst, results in charged particles, which can affect bed characteristics.

9. COLUMN MATERIAL

A few studies have examined the impact of column material on electrostatic phenomena in fluidized bed reactors [126, 160, 161], and it has been argued that column material alters the electrical potential in fluidized beds. Fotovat et al. [147] measured the entrainment flux and charge density in the freeboard of two stainless steel and acrylic columns. The two columns had different entrainment fluxes and charge densities under equivalent operating conditions. A study by Hou et al. [73] examined HDPE particle charging in steel and acrylic columns. HDPE particles acquired more charge in steel columns than in acrylic columns. This could be due to the wider triboelectric series distance between steel and polyethylene than between acrylic and polyethylene.

10. REACTOR START UP

It is believed that reactor wall sheeting occurs during the start-up period, about 12-72 hours after the beginning of the reaction or after production equivalent to 6–10 times the bed weight [4, 162,163]. During the start-up period, key variables change rapidly. Changes in catalyst co-monomer, monomer feed rates, or even temperature [to some extent] may be required to increase production and set product characteristics. Yamaguchi et al. [162] claimed that using a seedbed with particles containing moisture or molecular oxygen before initiating the polymerization reaction would effectively reduce sheeting after the reaction is initiated. Their claims apply to titanium- or vanadium-based catalysts used with an alkyl aluminum co-catalyst. They concluded that each bed has an optimum moisture content. Addition of water to a gas phase olefin polymerization reactor in amounts greater than 3 ppm V. permits an increase in the level of condensable gas and facilitates operation of the reactor at an elevated dew point by ameliorating electrostatic phenomena in the reactor; the process inhibits sheeting [164]. As addition of an alkyl compound (e.g. TEAL) to a seedbed during the reactor start-up procedure often generates negative charges due to the reaction with water in the bed. The reaction products of water with TEAL are thought to be responsible for generating an electrostatic charge. However, an extra amount of co-catalyst not only reduces catalyst activity but also contributes to charge generation.

11. CONCLUSION

Wall sheeting and fouling in fluidized bed reactors can cause many problems for industries. To control and eliminate fluidized bed electrification, a comprehensive understanding of triboelectric charging is essential. The purpose of this article was to explore the general concepts and effects of electrostatics on hydrodynamics, and vice versa. Effective parameters were explained to provide a thorough overview of the situation. They were also explained to be practical for engineers in the industry, and show how future studies should be focused more. Future studies suggested that working on turbulent flow on electrostatic effects of particles, the mechanism of triboelectric charging due to collision or friction between particle-particle and particle-reactor wall, the new antistatic materials and pneumatic conveying system, and investigating the effects of operational and structural parameters of fluidized bed reactors.

Nomenclature

q/m	Specific particle charges, defined as the particle charge-to-mass ratio or the net charge per unit mass
U_{mf}	minimum fluidization velocity [m/s]
U	Superficial gas velocity [m/s]
ρ_s	solid density
d_p	mean particle size
RH	Relative humidity
λ_D	Debye radius/distance
LDPE	Low density polyethylene
LLDPE	Linear Low-density polyethylene
HDPE	High density polyethylene

REFERENCES

[1] John G. Yates, Paola Lettieri. (2016). Fluidized-Bed Reactors: Processes and Operating Conditions, Volume 26.
[2] D. Kunii, O. Levenspiel. (1991). Fluidization Engineering, Buttenworth-Heinemann, Newton, USA.
[3] [A. Chen, H. Bi, J.R. Grace. (2006). Effects of probe numbers and arrangement on the measurement of charge distributions around a rising bubble in a two-dimensional fluidized bed. Chem. Eng. Sci., vol. 61, p. 6499-6510.
[4] G. Hendrickson. (2006). Electrostatics and gas phase fluidized bed polymerization reactor wall sheeting. Chem. Eng. Sci., vol. 61, p. 1041–64.
[5] M. Manafi, R. Zarghami, N. Mostoufi (2021). Charge transfer and bipolar charging of particles in a bubbling fluidized bed. Particuology, vo. 54, p.109-115.
[6] Joao B. P. Soares and Timothy F. L. McKenna. (2012). Polyolefin Reaction Engineering. ISBN: 978-3-527-31710-3.
[7] Burdett I D, Eisinger RS, Cai P, Lee KH. (2001). Gas-phase fluidization technology for production of polyolefins. In: Fluidization X. United Engineering Foundation, New York, p. 39–52.
[8] J. W. Lee, S.W. Kang, B. S. Chun, S. Jae. (2020). Olefin polymerization method using antistatic agent for metallocene olefin polymerization process. European Patent EP4019555A1.
[9] J. Wang, Y. Xu, W. Li, Y. Yang, F. Wang. (2009). Electrostatic potentials in gas-solid fluidized beds influenced by the injection of charge inducing agents. Electrostat, vol. 7, p. 815–826.
[10] Q. Zhao, X. Bi, P. Zhang, C. Liang. (2023). A study of charging characteristics of binary mixture of polyolefin particles by using horizontal airflow to separate large and small particles. Powder Technology, vol. 420, 118399.
[11] J. Lu, J. Yang, J. Qiao. (2023). Enhancement of electrostatic suppression in bubbling fluidized bed through carbon fiber addition. Powder Technology, vol. 428, 118797.
[12] R.Jaiswal, N.C.I.S. Furuvik, R.K. Thapa. (2020). Method of identifying an operating regime in a bubbling fluidized bed gasification reactor. Int. J. Energy Prod. Manag, vol. 5, p.24–34.
[13] W. C. Yang. (2003). Other nonconventional fluidized beds. In Handbook of Fluidizfition and Fluid-Particle Systems; Siemens Westinghouse Power Corporation: Pittsburgh, PA, USA.
[14] R. Cocco, J.W. Chew. (2023). 50 years of Geldart classification. Powder Technology, vol. 428, 118861.
[15] F. Johnsson, R. Zijerveld, J. Schouten, C.V.D. Bleek. (2000). Characterization of fluidization regimes by time-series analysis of pressure fluctuations. Int. J. Multiph. Flow, vol. 26, p. 663–715.
[16] R. Jaiswal, B. M. E. Moldestad, M.S. Eikeland, H.K. Nielsen, R.K. Thapa. (2022). Image Processing and Measurement of the Bubble Properties in a Bubbling Fluidized Bed Reactor. Energies, vol. 15, 7828.
[17] G. Rovero, M. Curti, G. Cavaglià. (2012). Optimization of Spouted Bed Scale-Up by Square-Based Multiple Unit Design. Advances in Chemical Engineering. DOI: 10.5772/33395
[18] D. Geldart. (1973). Types of gas fluidization. Powder Tecnology, vol. 7, p.285–292.

[19] J. Sun, Y. Yan. (2016). Non-intrusive measurement and hydrodynamics characterization of gas–solid fluidized beds: a review. Measurement Science and Technology, vol. 27.
[20] W. Fang, W. Jingdai, Y. Yongrong. (2008). Distribution of electrostatic potential in a gas–solid fluidized bed and measurement of bed level. Industrial & Engineering Chemistry Research, vol. 47, p. 9517–9526.
[21] F.S. Ali, M.A. Ali, R.A. Ali, I.I. Inculet. (1998). Minority charge separation in falling particles with bipolar charge. Journal of Electrostatics, vol. 45, p. 139–155.
[22] Q. Shi, Q. Zhang, J. Wang. (2017). Simultaneous measurement of electrostatic charge and its effect on particle motions by electrostatic sensors array in gas-solid fluidized beds. Powder Technology, vol. 312, p. 29-37.
[23] Y. Zhao, M. Liu, J. Yao. (2023). Electrostatics of granules and granular flows: A review. Advanced Powder Technology, vol. 34, 103895.
[24] F. Fotovat, X.T. Bi, J.R. Gracev. (2017). Electrostatics in Gas-Solid Fluidized Beds: A Review, Chemical Engineering Science, p. 303-334.
[25] P.Mehrani, H.T. Bi, J.R. Grace. (2004). Electrostatic charge generation in gas–solid fluidized beds. Recent Developments in Applied Electrostatics, p. 25-28.
[26] A. Sowinski, F. Salama, P. Mehrani. (2009). New technique for electrostatic charge measurement in gas–solid fluidized beds. Electrostatics, vol. 67, p. 568–573.
[27] A. Sowinski, L. Miller, P. Mehrani. (2010). Investigation of electrostatic charge distribution in gas–solid fluidized beds. Chemical Engineering Science, vol. 65, p. 2771–2781.
[28] K. S. Choi, K. T. Moon, J. H. Chung, X. Bi, J. R. Grace. (2011). Electrostatic hazards of polypropylene powders in the fluidized bed reactor. International Conference on Industrial Engineering and Engineering Management, p.995-999.
[29] X.T. Bi. (2011). Electrostatic phenomena in fluidization systems: Current status of understanding and future research needs, in: Knowlton. 10th Circulating Fluidized Bed and Fluidization Technology. ECI press, p. 41–57.
[30] D. Song, F. Salama, J. Matta, P. Mehrani. (2016). Implementation of Faraday cup electrostatic charge measurement technique in high-pressure gas–solid fluidized beds at pilot-scale. Powder Technology, vol. 290, p. 21-26.
[31] H. Wang, F. Fotovat, X.T Bi, J.R. Grace. (2019). Tribo-charging of binary mixtures composed of coarse and fine particles in gas–solid pipe flow. Particuology, vol. 43, p. 101-109.
[32] D. Song, P. Mehrani. (2017). Mechanism of particle build-up on gas-solid fluidization column wall due to electrostatic charge generation. Powder Technology, vol. 316, p. 166-170.
[33] A. Sowinski, A. Mayne, B. Javed, P. Mehrani, (2011). Comparison of the effect of grounding the column wall in gas- solid fluidized beds on electrostatic charge generation. J. Phys. Conf. Ser. 301.
[34] F. Salama, A. Sowinski, K. Atieh, K, P. Mehrani. (2013). Investigation of electrostatic charge distribution within the reactor wall fouling and bulk regions of a gas-solid fluidized bed. Electrostatics, vol. 71, p. 21– 27.
[35] Q. Zhang, K. Dong, Y. Zhou, Z. Huang, Z. Liao, F. Wang. (2016). A comparative study of electrostatic current and pressure signals in a MSFC gas-solid fluidized bed. Powder Technology, vol. 287, 292–300.
[36] A. Sowinski, A. Mayne, P. Mehrani. (2012). Effect of fluidizing particle size on electrostatic charge generation and reactor wall fouling in gas-solid fluidized beds. Chemical Engineering Science, vol. 71, p.552–563.
[37] A. Sowinski, L. Miller, P. Mehrani. (2010). Investigation of electrostatic charge distribution in gas-solid fluidized beds Chemical Engineering Science, vol. 65, p. 2771–2781.
[38] J. He, S. Huang, H. Chen, L. Zhu, B. Yang. (2023). Recent advances in the intensification of triboelectric separation and its application in resource recovery: A review. Chemical Engineering and Processing, vol. 45, 109308.
[39] H. Zhao, G.S.P. Castle, A.G. Bailey. (2003). Bipolar charging of poly-disperse polymer powders in fluidized beds. IEEE Transactions on Industry Applications, vol. 39(3), p. 612 - 618.
[40] P. Mehrani, H. T. Bi, J. R. Grace. (2007), Electrostatic behavior of different fines added to a Faraday cup fluidized bed. Electrostatics, vol. 65, p. 1–10.
[41] Alsmari, T.A., 2014. Effect of operating conditions and particle properties on electrostatics and entrainment in gas-solid fluidized beds, Ph.D. dissertation. University of British Columbia, Vancouver, Canada.

[42] F. Fotovat, J.R. Grace, X.T. Bi. (2016). Particle entrainment from gas-solid fluidized beds: conductive vs. dielectric fines. AIChE vol. 63, p. 1194–1202.
[43] P.Mehrani , M. Murtomaa , D.J. Lacks. (2017). An overview of advances in understanding electrostatic charge buildup in gas-solid fluidized beds. Electrostatics, vol. 87, p. 64-78.
[44] F. Chowdhury, M. Ray, A. Sowinski, P. Mehrani, A. Passalacqua. (2021). A review on modeling approaches for the electrostatic charging of particles. Powder Technology, vol. 389, p. 104-118.
[45] J Revel, Cendrine Gatumel, John A. Dodds, J Taillet. (2003). Generation of static electricity during fluidisation of polyethylene and its elimination by air ionisation. Powder Technology, vol. 135, p. 192-200.
[46] A. Chen, A., H.T. Bi, J.R. Grace. (2006). Measurement of charge distribution around a rising bubble in a 2-D fluidized bed. AIChE J. vol. 52, p. 174–184.
[47] A. Chen, A., H.T. Bi, J.R. Grace. (2007). Charge distribution around a rising bubble in a two-dimensional fluidized bed by signal reconstruction. Powder Technology, vol. 177, p. 113–124.
[48] K. Dong, Q. Zhang, Z. Huang, Z. Liao, J. Wang, Y. Yang. (2015). Experimental investigation of electrostatic effect on bubble behaviors in gas-solid fluidized bed. AIChE Journal, vol. 61[4], p. 1160–1171.
[49] J.R. Coombes, Y. Yan. (2015). Experimental investigations into the flow characteristics of pneumatically conveyed biomass particles using an electrostatic sensor array. Fuel vol. 151, p. 11–20.
[50] W. Zhang, Y. Yang, J. Wang. (2015). Measurement of flow parameters in a bubbling fluidized bed using electrostatic sensor arrays. Instrumentation and Measurement Technology Conference, p. 1573–1577.
[51] W.O. Moughrabiah, J.R. Grace, X.T. Bi. (2009). Effects of pressure, temperature, and gas velocity on electrostatics in gas–solid fluidized beds. Industrial & Engineering Chemistry Research, vol. 48, p. 320–325.
[52] Z.L. Liu, X.T. Bi, J.R. Grace. (2010). Electrostatic charging behavior of dielectric particles in a pressurized gas–solid fluidized bed. Electrostatics, vol. 68, p. 321–327.
[53] W.O. Moughrabiah, J.R. Grace, X.T. Bi. (2012). Electrostatics in gas–solid fluidized beds for different particle properties. Chemical Engineering Science, vol. 75, p. 198–208.
[54] C. He, J.R. Grace, X.T. Bi. (2015). Simultaneous measurements of particle charge density and bubble properties in gas–solid fluidized beds by dual-tip electrostatic probes. Chemical Engineering Science, vol.123, p. 11–21.
[55] C. He, J.R. Grace, X.T. Bi. (2016). Comparison of conventional and novel probes for measuring electrostatics and hydrodynamics during fluidization of polyethylene. Electrostatics, vol. 79, p. 7–15.
[56] S. Matsusaka, H. Maruyama, T. Matsuyama, M. Ghadiri. (2010). Triboelectric charging of powders: A review. Chemical Engineering Science, vol. 65, p. 5781–5807.
[57] B. Demirbas, J. Nijenhuis, C.U. Yurteri, J.R. Ommen. (2008). Towards monitoring electrostatics in gas–solid fluidized beds. Canadian Journal of Chemical Engineering, vol. 86, p. 493–505.
[58] D. Gidaspow, Y. Seo, B. Ettehadieh. (1983). Hydrodynamics of fluidization: experimental and theoretical bubble sizes in a two-dimensional bed with jet. Chem. Eng. Commun., vol. 22, p. 253–272.
[59] D.J. Lacks, R.M. Sankaran. (2011). Contact electrification of insulating materials. J. Phys. D. Appl. Phys., vol. 44, 453001.
[60] L. S. McCarty, G. M. Whitesides. (2008). Electrostatic charging due to separation of ions at interfaces: Contact Electrification of Ionic Electrets. Chem., Int. Ed, vol. 47, p. 2188−2207.
[61] X. Zhang, L. Chen, Y. Jiang, W. Lim, S. Soh. (2019). Rationalizing the Triboelectric Series of Polymers. Chemistry of Materials, vol. 31, p. 1473–1478.
[62] S. Pan, Z. Zhang. (2019). Fundamental theories and basic principles of triboelectric effect: A review. Friction, vol. 7, p. 2–17.
[63] N. Li, L. Ma, X. Xu, J. Luo. (2020). Charge transfer dynamics in contact electrification of dielectrics investigated by triboluminescence. Journal of Luminescence, vol. 227, 117531.
[64] M.W. Williams. (2012). Triboelectric charging of insulating polymers– some new perspectives. AIP Advances, vol.2, 010701.
[65] M.W. Williams. (2012). Triboelectric charging of insulators – mass transfer versus electrons/ions. Electrostatics, vol. 70, p. 233–234.
[66] U.G. Musa, S. Doruk Cezan, B. Baytekin, H. T. Baytekin. (2018). The Charging Events in Contact-Separation Electrification. Scientific Reports, vol. 8, 2472.
[67] A. Wang, D. Gil, M. Holonga, D.J. Lacks. (2017). Dependence of triboelectric charging behavior on

material microstructure. Phys Rev Mater, vol. 1, 035605.
[68] Y.G. Chung, D.J. Lacks. (2012). Atomic mobility in strained glassy polymers: The role of fold catastrophes on the potential energy surface. Polymer Science Part B, vol. 50, p. 1733–1739.
[69] Y.J. Kim, J. Lee, S. Park, C. Park, C. Park, H. Choi. (2017). Effect of the relative permittivity of oxides on the performance of triboelectric nanogenerators. RSC Advances, 28.
[70] Z. L. Wang, L. Lin, J. Chen, S. Niu, Y. Zi. (2016). Triboelectric Nanogenerators, Springer, Switzerland. ISBN: 978-3-319-40038-9.
[71] F. Chowdhury, M. Ray, A. Passalacqua, P. Mehrani, A. Sowinski. (2021). Electrostatic charging due to individual particle-particle collisions. Powder Technology, vol. 381, p. 352-365.
[72] M. Taghavivand, P. Mehrani, A. Sowinski. (2021). Triboelectric effects of a pneumatically injected silica catalyst support on polyethylene fluidized bed wall fouling. Powder Technology, vol. 385, p. 287-298.
[73] J. Hou, X. Liu, M. H. Rahman, H. Li, S. Sundaresan. (2023). Effect of gas properties and wall materials on particle charging in gas–solid fluidized beds. Canadian Journal of Chemical Engineering, vol. 101(1), p. 244-255.
[74] P. Mehrani, H.T. Bi, J. R. Grace. (2007). Bench-scale tests to determine mechanisms of charge generation due to particle–particle and particle–wall contact in binary systems of fine and coarse particles. Powder Technology, vol. 173, p. 73-81.
[75] F. Fotovat, X.T. Bi, J.R. Grace. (2018). A perspective on electrostatics in gas-solid fluidized beds: Challenges and future research needs. Powder Technology, vol. 329, p. 65-75.
[76] H.T. Bi. (2005). Electrostatic phenomena in gas-solids fluidized beds. China Particuology, vol. 3, p. 395–399.
[77] Q. Zhou, L. Li, Xi. Bi, G. Zhang, Z. Cao, H. Meng, Q. Lan, C. Liang, X. Chen, J. Ma. (2022). Electrostatic elimination of charged particles by DC-type bipolar electrostatic eliminator. Powder Technology, vol. 408, 117774.
[78] F. Salama, A. Sowinski, K. Atieh, P. Mehrani. (2013). Investigation of electrostatic charge distribution within the reactor wall fouling and bulk regions of a gas-solid fluidized bed. Electrostatics, vol. 71, p. 21– 27.
[79] C.F. Gallo, W.L. Lama. (1976). Classical electrostatic description of the work function and ionization energy of insulators. IEEE Trans. Ind. Appl, p. 7–11.
[80] A. Vitale, A. Alessandro, I. Stefano, C. Erwin, H. Arda. (2023). Devolatilization of Polypropylene Particles in Fluidized Bed. Energies, vol. 16, 6324.
[81] W. Fang, W. Jingdai, Y. Yongrong. (2008). Distribution of electrostatic potential in a gas-solid fluidized bed and measurement of bed level. Ind. Eng. Chem. Res., vol. 47, p. 9517–9526.
[82] K. Rahman, C. Campbell. (2002). Particle pressures generated around bubbles in gas fluidized beds. J. Fluid Mech., vol. 455, p. 103–127.
[83] A. Giffin, P. Mehrani. (2010). Comparison of influence of fluidization time on electrostatic charge buildup in the bubbling vs. slugging flow regimes in gas-solid fluidized beds. Electrostatics, vol. 68, p. 492–502.
[84] P. Tiyapiboonchaiya, D. Gidaspow, S. Damronglerd. (2012). Hydrodynamics of electrostatic charge in polypropylene fluidized beds. Ind. Eng. Chem. Res., vol.51, p. 8661–8668.
[85] J. Ji, H. Ji, L. Zhang, X. Zhao, X. Bai, X. Fan, F. Zhang, R.S. Ruoff. (2013). Graphene-encapsulated Si on ultrathin-graphite foam as anode for high-capacity lithium-ion batteries. Adv. Mater., vol. 25, p. 4673–4677.
[86] Z. Chen, J.W.F. To, C. Wang, Z. Lu, N. Liu, A. Chortos, L. Pan, F. Wei, Y. Cui, Z. Bao. (2014). A three-dimensionally interconnected carbon nanotube–conducting polymer hydrogel network for high performance flexible battery electrodes. Adv. Energy Mater., vol. 4, 1400207.
[87] C. Pei, C.Y. Wu, D. England, S. Byard, H. Berchtold, M. Adams. (2015). DEM-CFD modeling of particle systems with long-range electrostatic interactions. AIChE J., vol. 61, p. 1792–1803.
[88] T.A. Alsmari, J.R. Grace, X. T. Bi. (2016). Effects of particle properties on entrainment and electrostatics in gas–solid fluidized beds. Powder Technology, vol. 290, p. 2-10.
[89] D.J. Lacks, R.M. Sankaran. (2016). Triboelectric charging in single-component particle systems. Part. Sci. Technol., vol. 34, p. 55–62.
[90] A. Repoulias, I. Logothetis, D. Matsouka. (2023). Contact Area of Electrification Materials Relating to Triboelectric Generators: A Comparative Study. Electronic Materials Letters.
[91] P. Jiang, H. Bi, S. Liang, L.S. Fan. (1994). Hydrodynamic behavior of circulating fluidized bed with

polymeric particles. AIChE J., vol. 40, p. 193–206.
[92] J. Revel, C. Gatumel, J.A. Dodds, J. Taillet. (2003). Generation of static electricity during fluidization of polyethylene and its elimination by air ionisation. Powder Technology, vol. 135–136, p. 192–200.
[93] A. Wolny, W. Kaźmierczak. (1993). The influence of static electrification on dynamics and rheology of fluidized bed. Chemical Engineering Science, vol. 48, p. 3529–3534.
[94] Z. Tan, C. Liang, J. Li, S. Zhang. (2018). The effect of electrostatics on single bubble in fluidized bed and its mechanism analysis. Powder Technology, vol. 325, p. 545-556.
[95] A.S. Issangya, R.A. Cocco, S.R. Karri, T.M. Knowlton, J.W. Chew. (2022). Bed density and bubble void fraction variation in a fluidized bed stripper. Chemical Engineering Science, vol. 260, 117837.
[96] C.E. Agu, L.A. Tokheim, M. Eikeland, B.M. Moldestad. (2017). Determination of onset of bubbling and slugging in a fluidized bed using a dual-plane electrical capacitance tomography system. Chem. Eng. J., vol. 328, p. 997–1008.
[97] M. I. Nimvari, R. Zarghami, D. Rashtchian. (2020). Experimental investigation of bubble behavior in gas-solid fluidized bed. Advanced Powder Technology, vol. 31, p. 2680-2688.
[98] J. Delgado, M.P. Aznar, J. Corella. (1997). Biomass gasification with steam in fluidized bed: effectiveness of CaO, MgO, and CaO-MgO for hot raw gas cleaning. Ind. Eng. Chem. Res., vol. 36, p. 1535–1543.
[99] J. van der Schaaf, J.C. Schouten, F. Johnsson, C.M. Van den Bleek. (2002). Non-intrusive determination of bubble and slug length scales in fluidized beds by decomposition of the power spectral density of pressure time series. Int. J. Multiph. Flow, vol. 28, p. 865–880.
[100] Z. Peng, E. Doroodchi, B. Moghtaderi. (2020). Heat transfer modelling in Discrete Element Method (DEM)-based simulations of thermal processes: Theory and model development. Progress in Energy and Combustion Science, vol. 79, 100847.
[101] J.R. van Ommen, S. Sasic, J. Van der Schaaf, S. Gheorghiu, F. Johnsson, M.O. Coppens, Time-series analysis of pressure fluctuations in gas–solid fluidized beds–A review. (2011). Int. J. Multiph. Flow, vol. 37, p. 403–428.
[102] C. Vial, E. Camarasa, S. Poncin, G. Wild, N. Midoux, J. Bouillard. (2000). Study of hydrodynamic behaviour in bubble columns and external loop airlift reactors through analysis of pressure fluctuations. Chem. Eng. Sci., vol. 55, p. 2957– 2973.
[103] O. Winter. (1968). Density and pressure fluctuations in gas fluidized beds. AIChE J., vol. 14, p. 426–434.
[104] H.T. Bi, J.R. Grace, J. Zhu. (1995). Propagation of pressure waves and forced oscillations in gas-solid fluidized beds and their influence on diagnostics of local hydrodynamics. Powder Technology, vol. 82, p. 239–253.
[105] J. van der Schaaf, J.C. Schouten, C.M. Van den Bleek. (1998). Origin, propagation and attenuation of pressure waves in gas—solid fluidized beds.Powder Technology, vol. 95, p. 220–233.
[106] D. Musmarra, S. Vaccaro, M. Fillai, L. Massimilla. (1992). Propagation characteristics of pressure disturbances originated by gas jets in fluidized beds. Int. J. Multiph. Flow, vol. 18, p. 965–976.
[107] S. Sasic, B. Leckner, F. Johnsson. (2007). Characterization of fluid dynamics of fluidized beds by analysis of pressure fluctuations. Progress in Energy and Combustion Science, vol.33, p. 453–496.
[108] D. Musmarra, M. Poletto, S. Vaccaro, R. Clift. (1995). Dynamic waves in fluidized beds, Powder Technology, vol. 82, p. 255–268.
[109] H. Bi, A. Chen. (2003). Pressure fluctuations in gas-solids fluidized beds, China Particuology, vol. 1, p. 139–144.
[110] H.T. Bi. (2007). A critical review of the complex pressure fluctuation phenomenon in gas-solids fluidized beds. Chem. Eng. Sci., vol. 62, p. 3473–3493.
[111] C.R. Müller, J.F. Davidson, J.S. Dennis, P.S. Fennell, L.F. Gladden, A.N. Hayhurst, M.D. Mantle, A.C. Rees, A.J. Sederman. (2007). Oscillations in gas-fluidized beds: Ultrafast magnetic resonance imaging and pressure sensor measurements. Powder Technology, vol. 177, p. 87–98.
[112] C.M. Boyce, J.F. Davidson, D.J. Holland, S.A. Scott, J.S. Dennis. (2014). The origin of pressure oscillations in slugging fluidized beds: Comparison of experimental results from magnetic resonance imaging with a discrete element model. Chem. Eng. Sci., vol. 116, p. 611–622.
[113] L. Yao, H.T. Bi, A. Park. (2002). Characterization of electrostatic charges in freely bubbling fluidized beds with dielectric particles. Electrostatics, vol. 56, p. 183–197.
[114] F. Jalalinejad, X.T. Bi, J.R. Grace. (2012). Effect of electrostatic charges on single bubble in gas-solid fluidized beds. Int. J. Multiph. Flow, vol. 44, p. 15–28.

[115] M.A. Hassani, R. Zarghami, H.R. Norouzi, N. Mostouf. (2013). Numerical investigation of effect of electrostatic forces on the hydrodynamics of gas–solid fluidized beds. Powder Technology, vol. 246, p. 16-25.
[116] F. Jalalinejad, X.T. Bi , J.R. Grace. (2015). Effect of electrostatics on freely-bubbling beds of mono-sized particles. International Journal of Multiphase Flow, vol. 70, p. 104-112.
[117] F. Jalalinejad, X.T. Bi, J.R. Grace. (2016). Comparison of theory with experiment for single bubbles in charged fluidized particles. Powder Technology, vol. 290, p. 27-32.
[118] Ma. Manafi, R. Zarghami, N. Mostoufi. (2019). Effect of electrostatic charge of particles on hydrodynamics of gas-solid fluidized beds. Advanced Powder Technology, vol. 30(4), p. 815-828.
[119] M. Manafi, R. Zarghami, N. Mostoufi. (2019). Fluidization of electrically charged particles. Electrostatics, vol. 99, p. 9-18.
[120] J.W. Chew, A. Cahyadi, C.M. Hrenya, Re.Karri, R. Cocco. (2015). Review of entrainment correlations in gas–solid fluidization. Chemical Engineering Journal, vol. 260, p. 152-171.
[121] F. Fotovat, T.A. Alsmari, J.R. Grace, X.T. Bi. (2017). The relationship between fluidized bed electrostatics and entrainment. Powder Technology, vol. 316, p. 157-165.
[122] P. Zhang, C. Liang, Q. Zhou, X. Chen, J. Ma. (2021). Experimental investigation of particle adhesion on the wall due to electrostatic charge in gas-solid fluidized beds. Powder Technology, vol. 387, p. 373-384.
[123] T.A. Alsmari, J.R. Grace, X.T. Bi. (2015). Effects of superficial gas velocity and temperature on entrainment and electrostatics in gas–solid fluidized beds. Chemical Engineering Science, vol. 123, p. 49–56.
[124] J. Guardiola, V. Rojo, G. Ramos. (1996). Influence of particle size, fluidization velocity and relative humidity on fluidized bed electrostatics. Electrostatics, vol. 37, p. 1–20.
[125] A. Park, H. Bi, J.R. Grace. (2002). Reduction of electrostatic charges in gas-solid fluidized beds. Chemical Engineering Science, vol. 57, p. 153–162.
[126] J. Ciborowski, A. Wlodarski. (1962). On electrostatic effects in fluidized beds. Chemical Engineering Science, vol. 17, p. 23– 32.
[127] Y. Cheng, D.Y.J. Lau, G. Guan, C. Fushimi, A. Tsutsumi, C.H. Wang. (2012). Experimental and numerical investigations on the electrostatics generation and transport in the downer reactor of a triple-bed combined circulating fluidized bed. Ind. Eng. Chem. Res., vol. 51, p. 14258–14267.
[128] Y. Cheng, E.W.C. Lim, C.H. Wang, G. Guan, C. Fushimi, M. Ishizuka, A. Tsutsumi. (2012). Electrostatic characteristics in a large-scale triple-bed circulating fluidized bed system for coal gasification. Chem. Eng. Sci., vol. 75, p. 435–444.
[129] V. C. R. Eppala, M. M. Varghese, T. R. Vakamalla. (2023). Effect of particle shape on the hydrodynamics of gas-solid fluidized bed. Chemical Engineering Research and Design, vol. 189, p. 461-473.
[130] D. Boland, D. Geldart. (1972). Electrostatic charging in gas fluidized beds. Powder Technology vol. 5, p. 289-297.
[131] X. Yu, W. Li, Y. Xu, J. Wang, Y. Yang. (2010). Effect of polymer granules on the electrostatic behavior in gas-solid fluidized beds. Industrial & Engineering Chemistry Research, vol. 49, p.132–139.
[132] K. Kato, J. Li. (2001). A correlation of elutriation rate constant for adhesion particles [group C particles]. Powder Technology, vol. 118, p. 209–218.
[133] T. Nakazato, J. Li, K. Kato. (2004). Effect of cohesive powders on the elutriation of particles from a fluid bed. Chemical Engineering Science, vol. 59, p. 2777–2782.
[134] J. Baeyens, D. Geldart, S.Y. Wu. (1992). Elutriation of fines from gas fluidized bed of Geldart A-type powders-effect of adding superfines. Powder Technology, vol. 71, p. 71–80.
[135] Y. Tian, P. Mehrani. (2015). Effect of particle size in fluidization of polyethylene particle mixtures on the extent of bed electrification and wall coating. Electrostatics, vol. 76, p. 138-144.
[136] F. Aida, S. Wang, M. Fujita, G. Tanimoto, Y. Fujiwara. (1997). Study of the mechanism of space charge formation in polyethylene. Electrostatics, vol.42, p. 3–15.
[137] S. Matsusaka, M. Oki, H. Masuda. (2003). Bipolar charge distribution of a mixture of particles with different electrostatic characteristics in gas–solids pipe flow. Powder Technology, vol. 135–136, p. 150–155.
[138] D. Song, P. Mehrani. (2017). Effect of Fluidization Pressure on Electrostatic Charge Generation of Polyethylene Particles, Ind. Eng. Chem. Res., vol. 56, p. 14716−14724.
[139] M.I. Nimvari, A. Sowinski, P. Mehrani. (2022). Effect of temperature on triboelectrifcation of

polyethylene particles in a pilot-scale pressurized gas-solid fluidized bed. Powder Technology, vol. 405, 117524.
[140] G. Tardos, R. Pfeffer, M. Peters, T. Sweeney. (1983). Filtration of airborne dust in a triboelectrically charged fluidized bed. Industrial and Engineering Chemistry Fundamentals vol. 22, p. 445–453.
[141] W. W. Kazmierczak. (1989). Triboelectrification in fluidized bed of polystyrene. Chemical Engineering Science, vol. 44, p. 2607–2610.
[142] A. Chen, H.T. Bi, J.R. Grace. (2003). Measurement of particle charge-to-mass ratios in a gas-solids fluidized bed by a collision probe. Powder Technology, vol. 135–136, p. 181–191.
[143] A. Giffin, P. Mehrani. (2013). Effect of gas relative humidity on reactor wall fouling generated due to bed electrification in gas-solid fluidized beds. Powder Technology, vol. 235, p. 368–375.
[144] E. Németh, V. Albrecht, G. Schubert, F. Simon. (2003). Polymer tribo-electric charging: dependence on thermodynamic surface properties and relative humidity. Electrostatics, vol. 58, p. 3–16.
[145] T. Nomura, T. Satoh, H. Masuda. (2003). The environment humidity effect on the tribo-charge of powder. Powder Technology, vol. 135–136, p. 43–49.
[146] R. Sharma, S. Trigwell, A.S. Biris, R.A. Sims, M.K. Mazumder. (2003). Effect of ambient relative humidity and surface modification on the charge decay properties of polymer powders in powder coating. IEEE Trans. Ind. Appl., vol. 39, p. 87–95.
[147] F. Fotovat, K. Gill, J.R. Grace, X. T. Bi. (2017). Impact of column material on electrostatics and entrainment of particles from gas-solid fluidized beds. Chemical Engineering Science, vol. 167, p. 120-134.
[148] A. Schella, S. Herminghaus, M. Schroter. (2017). Influence of humidity on tribo-electric charging and segregation in shaken granular media. Soft Material, vol. 13, p. 394–401.
[149] J. Kolehmainen, P. Sippola, O. Raitanen, A. Ozel, C.M. Boyce, P. Saarenrinne. (2017). Effect of humidity on triboelectric charging in a vertically vibrated granular bed: experiments and modeling. Chemical Engineering Science, vol. 173, p.363–373.
[150] P. Sippola, J. Kolehmainen, A. Ozel, X. Liu, P. Saarenrinne, S. Sundaresan. (2018). Experimental and numerical study of wall layer development in a tribocharged fluidized bed. Journal of Fluid Mechanics, vol. 849, p. 860-884.
[151] R. D. Cruise, K. Hadler, S.O. Starr, J.J. Cilliers. (2022). The effect of particle size and relative humidity on triboelectric charge saturation. Journal of Physics D: Applied Physics, vol. 55(18).
[152] A. Sowinski, P. Mehrani. (2015). Impact of Addition of a Catalyst or Its Support on Reactor Wall Coating Due to Electrostatic Charging during Fluidization of Polyethylene. Ind. Eng. Chem. Res., vol. 54, p. 3981−3988.
[153] S. Mihan, A.Lange, W. Rohde. (2000). Solid reactor with an antistatic coating for carrying out reactions in a gaseous phase. patent WO2000007716A1.
[154] C. He, X.T. Bi, J.R. Grace. (2015). Monitoring Electrostatics and Hydrodynamics in Gas−Solid Bubbling Fluidized Beds Using Novel Electrostatic Probes. Ind. Eng. Chem. Res., vol. 54, p. 8333−8343.
[155] M. Taghavivand, A. Sowinski, P. Mehrani. (2021). Triboelectric effects of continuity additives and a silica catalyst support on polyethylene fluidized bed wall fouling. Chemical Engineering Science, vol. 245, 116882.
[156] J. Taillet. (1997). Applications of supersonic injection of electric charges in chemical engineering, Electrostatics, vol.40&41, p. 265-270.
[157] J. Taillet. (2003). Static charge elimination on polymer particulates during their industrial production: supersonic injection technology, Powder Technology, vol. 135–136, p. 201–208.
[158] M. Kachi, M. Nemamcha, H. Lazhar, L. Dascalescu. (2011). Neutralization of charged insulating granular materials using AC corona discharge, Electrostatics vol. 69, p. 296-301.
[159] K. Dong, Q. Zhang, Z. Huang, Z. Liao, J. Wang, Y. Yang. (2014). Experimental investigation of electrostatic reduction in a gas – solid fluidized bed by an in-situ corona charge eliminator. Industrial & Engineering Chemistry Research, vol. 53, p. 14217–14224.
[160] M. Fujino, S. Ogata, H. Shinohara. (1985). The electric potential distribution profile in a naturally charged fluidized bed and its effects. Industrial & Engineering Chemistry Research, vol. 25, p. 149–159.
[161] B.D. Fulks, S.P. Sawin, C.D. Aikman, J.M. Jenkins. (1989). Process for reducing sheeting during polymerization of alpha-olefins. US Patent 4,876,320, Assigned to Union Carbide Chemicals and Plastics Company Inc.

[162] Y. Yamaguchi, S. Suga, M. Morikawa, K. Kubo, M. Watanabe, Y. Sano. (1995). Method for producing polyolefin. US Patent 5,385,991, Assigned to Nippon Petrochemicals Company, Ltd.
[163] J.R. Chirillo, K.C. Kimbrough II, P.E. McHattie. (1989). Method for reducing sheeting during polymerization of alpha-olefins. US Patent 4,855,370, Assigned to Union Carbide Corporation,
[164] M. G. Goode, C.C. Williams, F. D. Hussein, T. J. McNeil, K.H. Lee. (1998). Static control in olefin polymerization. US Patent 6111034A, Assigned to Union Carbide Chemicals & Plastics Technology Corporation.
[165] A. A. Park, L. Fan. (2007). Electrostatic charging phenomenon in gas–liquid–solid flow systems. Chemical Engineering Science, vol. 62, p. 371-386.